J Physiol 591.23 (2013) pp 5977–5998

The Journal of Physiology

Oxygen and mitochondrial inhibitors modulate both monomeric and heteromeric TASK-1 and TASK-3 channels in mouse carotid body type-1 cells

Philip J. Turner and Keith J. Buckler

Department of Physiology, Anatomy and Genetics, University of Oxford, Oxford, UK

Key points

- TASK-like background potassium channels play a key role in the sensing of hypoxic, metabolic and acidic stimuli in arterial chemoreceptor cells.
- In this study, we investigated the roles of TASK-1 and TASK-3 in forming these channels by using gene deletion in mice.
- Deletion of *Task-1* (*Kcnk3*) and/or *Task-3* (*Kcnk9*) disrupted the main form of background K-channel activity.
- In single knock-out mice, we observed, instead of the wild-type channel, the homomeric forms of TASK-1 in *Task-3*$^{-/-}$ and TASK-3 in *Task-1*$^{-/-}$.
- All forms of TASK were inhibited by hypoxia, cyanide and the uncoupler FCCP.
- We conclude that the main form of background K-channel in chemoreceptor cells is a TASK-1/TASK-3 heterodimer and that both TASK-1 and TASK-3 subunits can couple to both oxygen and metabolic signalling pathways in these cells.

Abstract In rat arterial chemoreceptors, background potassium channels play an important role in maintaining resting membrane potential and promoting depolarization and excitation in response to hypoxia or acidosis. It has been suggested that these channels are a heterodimer of TASK-1 and TASK-3 based on their similarity to heterologously expressed TASK-1/3 fusion proteins. In this study, we sought to confirm the identity of these channels through germline ablation of *Task-1* (*Kcnk3*) and *Task-3* (*Kcnk9*) in mice. Background K-channels were abundant in carotid body type-1 cells from wild-type mice and comparable to those previously described in rat type-1 cells with a main conductance state of 33 pS. This channel was absent from both *Task-1*$^{-/-}$ and *Task-3*$^{-/-}$ cells. In its place we observed a larger (38 pS) K^+-channel in *Task-1*$^{-/-}$ cells and a smaller (18 pS) K^+-channel in *Task-3*$^{-/-}$ cells. None of these channels were observed in *Task-1*$^{-/-}$/*Task-3*$^{-/-}$ double knock-out mice. We therefore conclude that the predominant background K-channel in wild-type mice is a TASK-1/TASK-3 heterodimer, whereas that in *Task-1*$^{-/-}$ mice is TASK-3 and, conversely, that in *Task-3*$^{-/-}$ mice is TASK-1. All three forms of TASK channel in type-1 cells were inhibited by hypoxia, cyanide and the uncoupler FCCP, but the greatest sensitivity was seen in TASK-1 and TASK-1/TASK-3 channels. In summary, the background K-channel in type-1 cells is predominantly a TASK-1/TASK-3 heterodimer. Although both TASK-1 and TASK-3 are able to couple to the oxygen and metabolism sensing pathways present in type-1 cells, channels containing TASK-1 appear to be more sensitive.

(Resubmitted 15 July 2013; accepted after revision 10 September 2013; first published online 16 September 2013)

Corresponding author K. J. Buckler: Department of Physiology, Anatomy and Genetics, University of Oxford, Parks Road, Oxford OX1 3PT, UK. Email: keith.buckler@dpag.ox.ac.uk

Abbreviations AMPK, adenosine monophosphate activated protein kinase; E_K, equilibrium potential for K^+ ions; FCCP, carbonyl cyanide 4-(trifluoromethoxy)phenylhydrazone; GABA (A), γ-aminobutyric acid ligand-gated ion channel. K_B-channel, background K^+ channel; nPopen, estimated channel open probability; P_{O_2}, partial pressure of oxygen; TASK, TWIK-related acid-sensitive K^+ channel; TEA, tetraethylammonium; TRAAK, TWIK-related arachidonic-acid-stimulated K^+ channel; TREK, TWIK-related K^+-channel; TWIK, tandem of p domains in a weak inward rectifying K^+ channel; V_p, pipette potential; 4-AP, 4-aminopyridine.

DOI: 10.1113/jphysiol.2013.262022

Introduction

TASK-like potassium channels are thought to play a central role in mediating the excitatory response of arterial chemoreceptors to hypoxia, acidosis and hypercapnia (Buckler *et al.* 2000). Their presence in carotid body chemoreceptor cells was first suggested based on biophysical and pharmacological similarities between cloned TASK channels in heterologous expression systems and a native oxygen- and acid-sensitive background potassium current found in rat carotid body type-1 cells (Buckler, 1997; Buckler *et al.* 2000). The channels responsible for mediating this background current (originally termed 'K_B-channels') are very abundant in the type-1 cell membrane and share a number of characteristics with TASK channels, including minimal voltage sensitivity, acid sensitivity, resistance to the classical K-channel inhibitors TEA and 4-AP, and the ability to be activated by halothane. It was originally suggested that K_B-channels might be comprised of TASK-1, and TASK-1 mRNA was shown to be present in type-1 cells (Buckler *et al.* 2000). Further, more detailed, biophysical studies of K_B-channels, together with the cloning and characterization of another closely related member of the TASK channel family, TASK-3 (Chapman *et al.* 2000; Kim *et al.* 2000; Rajan *et al.* 2000), revealed some subtle differences between K_B-channels and TASK channels, principally relating to the magnesium sensitivity of single-channel conductance. These differences led us to speculate that the native channel might be a heteromer of TASK-1 and TASK-3 (Williams & Buckler, 2004) as TASK-3 was also reported to be expressed in type-1 cells (Yamamoto *et al.* 2002).

TASK channels belong to the tandem-p-domain K-channel (K2P) family, which possesses two pore-forming domains, each of which is sandwiched between two membrane-spanning domains in a tandem repeat (Goldstein *et al.* 1996; Lesage *et al.* 1996*a*). The functional form of K2P channels is believed to be dimeric (Lesage *et al.* 1996*b*; Brohawn *et al.* 2012; Miller & Long, 2012). The first suggestions of heterodimerization among some members of this family of channels were based on the pharmacological properties of whole cell currents produced in heterologous expression systems containing both TASK-1 and TASK-3 (Czirjak & Enyedi, 2002). Single-channel recordings of heteromultimeric channels formed in heterologous expression systems have never been reported, but fusion protein constructs (TASK-1–TASK-3 and TASK-3–TASK-1) expressed in heterologous systems generate TASK-like currents (Czirjak & Enyedi, 2002; Kang *et al.* 2004) and display single-channel properties which more closely resemble the predominant form of native K_B-channel activity in type-1 cells than either TASK-1 or TASK-3 alone (Kim *et al.* 2009). Thus, the current hypothesis is that the background K-channels in type-1 cells are predominantly TASK-1/TASK-3 heterodimers and include a small number of homomeric TASK-1 and TASK-3.

Defining the structure of native channels in the carotid body is important in a number of respects, but first and foremost investigations into the regulation of these channels by natural stimuli will ultimately depend upon the identification of regulatory motifs that couple to the relevant sensory transduction pathway. Before this can be achieved, it is necessary to confirm the channel's identity. For example, recent investigations into the mechanisms of oxygen sensing in these cells have focused upon a role for metabolism in which mitochondrial ATP formation may be linked to the control of channel activity via AMP kinase (Evans *et al.* 2005; Wyatt & Evans, 2007). Interestingly, however, it has been suggested that only TASK-3 is regulated by AMP kinase and that TASK-1 is not (Dallas *et al.* 2009).

In this study, we therefore sought to: (i) investigate the role of *Task-1* (*Kcnk3*) and *Task-3* (*Kcnk9*) genes in the formation of background K-channels in type-1 cells, and (ii) test the sensitivity of the different forms of channel possible (TASK-1, TASK-3 and TASK-1/TASK-3) to modulation by hypoxia and inhibitors of mitochondrial metabolism.

Methods

Animals

The *Task-1*$^{-/-}$ and *Task-3*$^{-/-}$ mice used in these studies have been described in detail elsewhere (Aller *et al.* 2005; Brickley *et al.* 2007). For both *Task-1*$^{-/-}$ and *Task-3*$^{-/-}$, the first coding exons are disrupted and no mutant allele is transcribed. *Task-1*$^{-/-}$/*Task-3*$^{-/-}$ double knock-out animals were produced by crossing the two single knock-out lines (Trapp *et al.* 2008). Although *Task-1*$^{-/-}$ and *Task-3*$^{-/-}$ have been described as mostly of the C57BL/6 strain, we identified animals with wild-type alleles produced during our *Task-1*$^{-/-}$ and *Task-3*$^{-/-}$ crossing programme, which were subsequently mated to generate the control (wild-type) line used in these experiments. Genotypes were confirmed by PCR of genomic DNA extracted from ear biopsies. All procedures involving animals were approved by the University of Oxford's Local Ethical Review Process and were conducted in accordance with project and personal licences issued under the UK Animals (Scientific Procedures) Act 1986.

Type-1 cell isolation

Carotid bodies were excised from young mice (aged 4–8 weeks) under terminal anaesthesia (2–4% halothane) in accordance with project and personal licences

issued under the UK Animals (Scientific Procedures) Act 1986. Type-1 cells were isolated using enzymatic dissociation with 0.25 mg ml^{-1} trypsin (Sigma-Aldrich Ltd, Gillingham, Dorset, UK) and 1.75 mg ml^{-1} collagenase P (Roche Diagnostics Ltd, Burgess Hill, West Sussex, UK) in Hank's balanced salt solution (HBSS) (pre-equilibrated with 5% CO_2, 11% O_2 air) for 25 min at 37°C. Tissue was subsequently transferred to enzyme-free culture medium and triturated through fire-polished pipettes. This cell suspension was plated out onto coverslips coated with a 20:1 mixture of poly-L-lysine and laminin (Sigma-Aldrich Ltd), which were incubated at 37°C for 2 h before additional culture medium was added. Culture medium comprised Ham's F-12 supplemented with 10% heat-inactivated fetal bovine serum, 2 mM L-glutamine and 4 μg ml^{-1} insulin. Cell isolates were used within 8 h.

Electrophysiology

Cell-attached patch clamp recordings were performed using an Axopatch 200B (Molecular Devices LLC, Sunnyvale, CA, US). Pipettes were fabricated from borosilicate glass capillaries (Harvard Apparatus Ltd, Kent, UK) and were sylgard-coated and fire-polished immediately before use. Cell-attached filling solution contained 140 mM KCl, 1 mM $MgCl_2$, 1 mM EGTA, 10 mM Hepes, 10 mM tetraethylammonium and 5 mM 4-aminopyridine. The pH of the filling solution was adjusted to 7.4 at 37°C. All single-channel recordings were carried out in high K^+ (100 mM K^+), nominally Ca^{2+}-free solutions (detailed below).

Single-channel recordings were filtered at 2–5 kHz and current was recorded and digitalized at 20 kHz. Voltage clamp control, data acquisition and analysis were performed using Spike2 4.21 (Cambridge Electronic Design, Cambridge, UK). Single-channel activity was defined by nP_{open}. Main conductance states for channel activity were established in an all-points histogram and used to set a 50% open threshold for nP_{open} definition analysis. Current levels which exceeded 150% of the main conductance state were classed as multiple openings.

Measurement of $[Ca^{2+}]_i$

Intracellular calcium measurements were performed using Indo-1 and a microspectrofluorimeter based on a Nikon Diaphot 200 (Nikon Corp., Tokyo, Japan) equipped with a xenon lamp to provide an excitation light source and cooled (−20°C) photomultiplier tubes (PMT; Thorn EMI, London, UK) to detect emitted fluorescence. Indo-1 was loaded into cells by incubation with 2–5 μM of the acetoxymethyl ester derivative in culture medium for 1 h at room temperature. Indo-1 was excited at 340 nm and fluorescence intensity measured at 405 ± 16 nm and 495 ± 10 nm. The fluorescence emission ratio (405:495) for Indo-1 was calibrated as previously described (Buckler & Vaughan Jones, 1993).

Solutions

Standard HCO_3^- buffered Tyrode solution contained 117 mM NaCl, 4.5 mM KCl, 2.5 mM $CaCl_2$, 1 mM $MgCl_2$, 23 mM $NaHCO_3$ and 11 mM glucose. High K^+ Tyrode contained 100 mM KCl, 21.5 mM NaCl, 1 mM $MgCl_2$, 23 mM $NaHCO_3$ and 11 mM glucose. Normoxic solutions were equilibrated with 5% CO_2 and 95% air; hypoxic solutions were equilibrated with 5% CO_2 and 95% N_2 (P_{O_2} = 2 Torr). Both standard and high K^+ Tyrode were pH 7.4 at 37°C.

Solutions containing NaCN were bubbled for > 15 min with 5% CO_2 95% air prior to the addition of the compound. NaCN was added immediately before use and solutions were subsequently maintained under an atmosphere of 5% CO_2 95% air to reduce loss of volatile HCN from solutions. Tyrodes containing NaCN were replaced with fresh solutions after approximately 1 h of experimentation.

Results

Standard recording conditions

Cell-attached patch recordings were performed on isolated type-1 cells perfused with 100 mM K^+ HCO_3^- buffered Tyrode and a pipette solution containing 140 mM K^+, plus 10 mM TEA and 5 mM 4-AP (see Methods for full composition). Pipette potential (V_p) was set at +80 mV for most recordings (unless otherwise indicated). These recording conditions were chosen so that: (i) any actions of hypoxia or metabolic inhibitors upon background K current would have minimal effect on cell membrane potential (estimated to be equivalent to $E_K = -9$ mV) so that a constant potential across the cell-attached patch of approximately −89 mV could be maintained under all conditions, and (ii) voltage-activated and Ca^{2+}-activated K^+-channels in the patch would be largely inhibited by the inclusion of TEA and 4-AP and the negative patch potential.

Background K^+-channel activity in wild-type mouse type-1 cells

Recordings from the type-1 cells of wild-type animals conducted under the conditions described above routinely displayed brief flickery inward currents. Analysis of these recordings revealed one main conductance level with a mean ± standard error of the mean (S.E.M.) amplitude of 2.51 ± 0.04 pA (n = 25). Other less frequent lower and

higher conductance levels were also observed in most patches consistent with unresolved partial openings of channels and the presence of multiple channels (Fig. 1*A* and *B*). Despite the appearance of variable conductance levels, the majority of patches showed only a single peak when analysed by all-points histograms (Fig. 1*D*). Occasionally, however, a second peak or shoulder of lower amplitude was also resolved, at approximately 1.3 pA (Fig. 1*C*).

Channels were active instantaneously and did not run down or inactivate over time. The most frequently observed channels were characterized by flickery kinetics with a mean ± S.E.M. nP_{open} of 0.20 ± 0.04 ($n = 30$) (the main conductance state as determined from all-points histograms was used to set a 50% threshold level for the determination of nP_{open}). The current–voltage (I–V) relationship of the main conductance level for inward currents was linear between 20 mV and 100 mV V_p, with a mean ± S.E.M. slope conductance of 33.4 ± 0.7 pS ($n = 15$) (Fig. 1*E*). The generally noisy nature of data recorded at negative pipette potentials precluded the sensible estimation of slope conductance of outward currents, but the reversal potential estimated by linear regression was at a V_p of approximately 4 mV. This is consistent with a potassium conductance.

The channels described above display properties similar to those of the background TASK-like potassium channels previously described in rat type-1 cells (see Discussion). It has been proposed that these background channels are probably formed from a TASK-1/TASK-3 heterodimer in rat type-1 cells with the possible co-presence of a small number of TASK-1 and TASK-3 homodimers (Kim *et al.* 2009). We sought to test this hypothesis using germline ablation of *Task-1* and *Task-3* genes.

Channel activity in *Task-1*$^{-/-}$ and *Task-3*$^{-/-}$ mouse type-1 cells

Cell-attached recordings from both *Task-1*$^{-/-}$ and *Task-3*$^{-/-}$ type-1 cells were performed under the same conditions as those used to study background K^+-channel activity in wild-type cells (see above).

Most cell-attached recordings in type-1 cells from *Task-1*$^{-/-}$ mice also displayed spontaneous channel activity that did not run down over time (Fig. 2*A*). Channel openings had a flickery appearance similar to that seen in channels from wild-type cells, but all-points histograms resolved only a single, well-defined peak with a mean ± S.E.M. amplitude of 3.31 ± 0.07 pA ($n = 29$) (Fig. 2*B*), which was significantly larger ($P < 0.0001$, unpaired two-tailed Student's t test) than that seen in wild-type cells. Channel activity was, however, significantly lower than in patches from wild-type cells, with a mean ± S.E.M. nP_{open} of only 0.008 ± 0.002 ($n = 21$; $P < 0.001$, unpaired two-tailed t test). Single-channel currents in *Task-1*$^{-/-}$ cells showed inward rectification with mean slope conductance values calculated from the I–V relationship of 37.6 ± 0.8 pS for inward currents ($n = 13$) (Fig. 2*C*). The estimated reversal potential for single-channel currents was at $V_p = -6.4$ mV, consistent with a potassium channel.

Background channel activity was also evident in cell-attached patches from *Task-3*$^{-/-}$ type-1 cells (Fig. 2*D*), but was of significantly lower amplitude than either wild-type or *Task-1*$^{-/-}$ channel currents ($P < 0.0001$ and $P < 0.0001$, respectively, unpaired two-tailed t test). Currents recorded at +80 mV V_p had a mean ± S.E.M. amplitude of 1.24 ± 0.05 pA ($n = 19$) for the principle peak and some other much less frequent higher conductance levels were also present, as determined by the all-points histogram (Fig. 2*E*). Channel kinetics were also flickery, with a relatively low mean ± S.E.M. nP_{open} of 0.047 ± 0.032 ($n = 17$), which was significantly lower than that in the wild-type ($P < 0.02$). *Task-3*$^{-/-}$ channels were instantaneously active and activity did not run down with time. The I–V relationship of inward currents between 60 mV and 100 mV V_p yielded a mean ± S.E.M. slope conductance of 18 ± 0.21 pS ($n = 5$). An unfavourable signal:noise ratio at more negative pipette potentials precluded an estimation of outward conductance. Current reversal was estimated by linear regression to be at $V_p = 7.1$ mV.

Channel activity in *Task-1*$^{-/-}$/*Task-3*$^{-/-}$ (double knock-out) type-1 cells

Background channel activity was infrequently observed in cell-attached patches in type-1 cells from *Task-1*$^{-/-}$/*Task-3*$^{-/-}$ double knock-out animals. In 20 patches recorded, a large conductance channel with flickery kinetics was recorded on four occasions (Fig. 3*A*). Single-channel currents at +80 mV V_p had a mean ± S.E.M. amplitude of 7.5 ± 0.8 pA ($n = 3$), as determined by an all-points histogram (Fig. 3*B*). The I–V relationship for inward currents between 20 mV and 100 mV V_p gave a mean ± S.E.M. slope conductance of 108 ± 4.8 pS ($n = 2$). In one recording channel, activity appeared to be inhibited by hypoxia; however, this was not replicable in the other three patches tested.

Another channel of far smaller conductance was also observed in three patches. This channel was characterized by long, stable, open states (Fig. 3*D*). Currents recorded at +80 mV V_p were approximately 0.6 pA in amplitude as determined by an all-points histogram (Fig. 3*E*). Because of the low frequency of occurrence of channels in *Task-1*$^{-/-}$/*Task-3*$^{-/-}$ type-1 cell patches, they were not studied further.

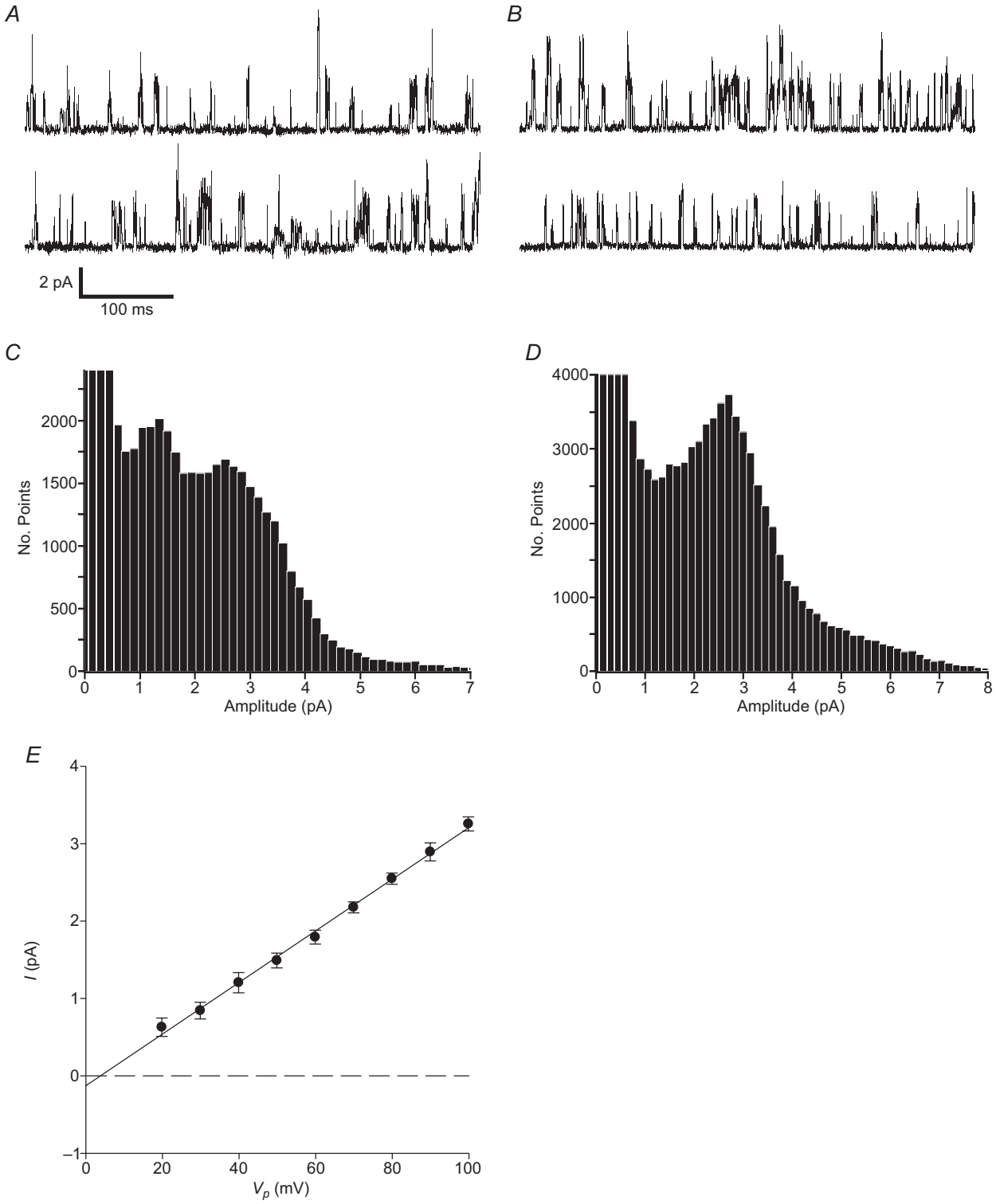

Figure 1. Background channel activity in cell-attached wild-type patches
A, *B*, cell-attached recordings from different type-1 cells, each with two contiguous sections of 500 ms in length. Upward deflections represent inward currents (open channel events with current flow into the cell). Cells were superfused with 100 mM K^+ Tyrode, with 140 mM K^+ in the pipette solution. Pipette potential (V_p) was +80 mV. *C*, *D*, all-points histograms (150 fA bin widths) generated from 10 s segments of cell-attached recordings under control conditions from the same cells as in *A* and *B*. *E*, mean single-channel current–voltage relationship (*I*–*V*) for background channel activity ($n = 15$). Mean data from inward currents were fitted by least squares linear regression and yielded a mean ± S.E.M. slope conductance of 33.4 ± 0.7 pS ($r^2 = 0.997$).

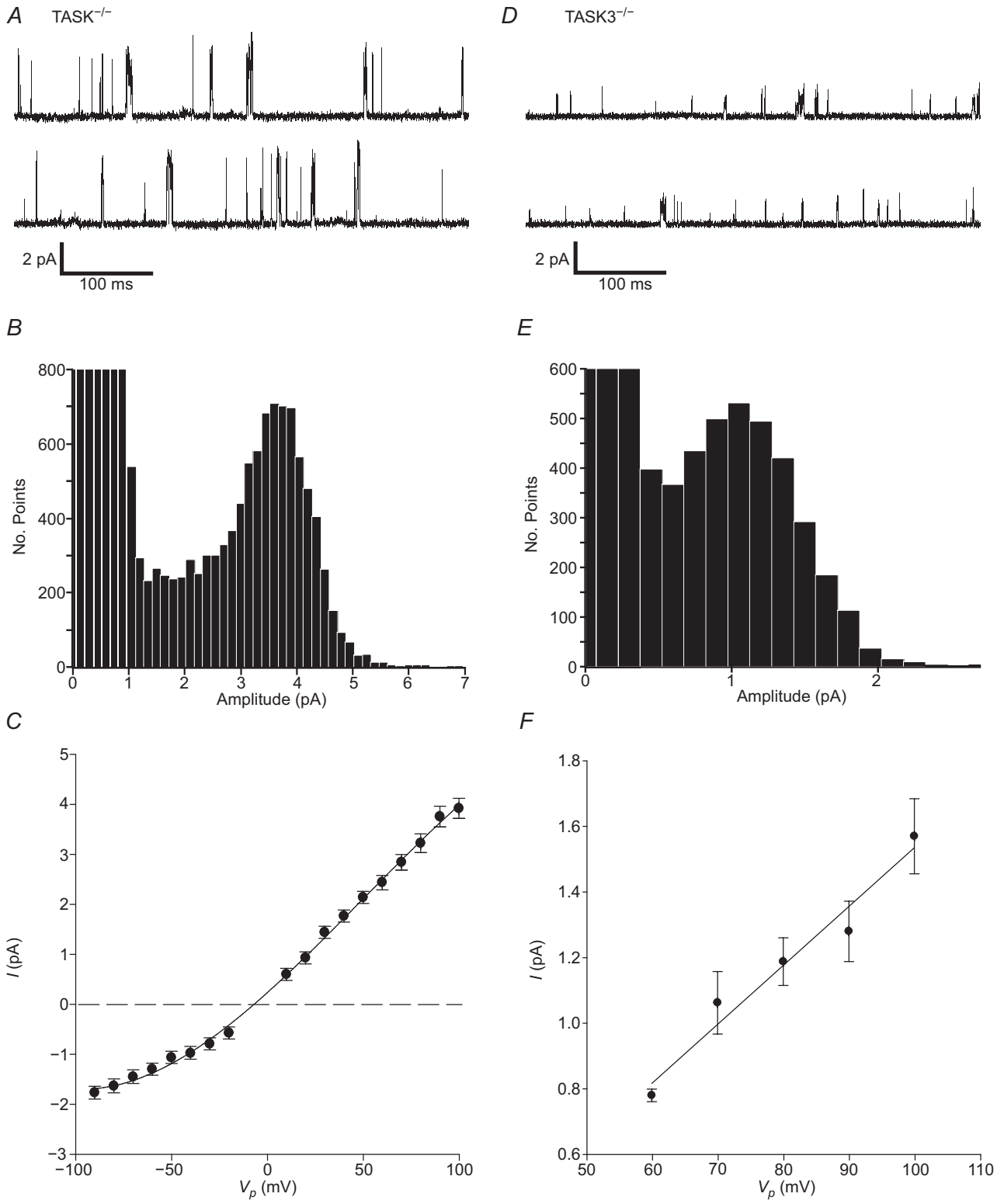

Figure 2. Background channel activity in cell-attached *Task-1*$^{-/-}$ and *Task-3*$^{-/-}$ patches
A, *D*, cell-attached recording of background channel activity from *Task-1*$^{-/-}$ and *Task-3*$^{-/-}$ type-1 cells respectively, each showing two contiguous 500 ms sections of recording. Recording conditions were as described for wild-type, type-1 cells. *B*, *E*, all-points histograms generated from 20 s and 40 s segments of cell-attached recordings for *Task-1*$^{-/-}$ and *Task-3*$^{-/-}$ type-1 cells, respectively. Bin widths were 150 fA. *C*, mean current–voltage (*I–V*) relationship for background channel activity in *Task-1*$^{-/-}$ type-1 cells ($n = 13$ for most points). Data for inward

Comparison of K^+-channels in wild-type, *Task-1*$^{-/-}$ *and Task-3*$^{-/-}$ type-1 cells

Mean nP_{open} values for channel activity in wild-type and Task knock-out animals were compared using an unpaired *t* test. Channel activity in wild-type animals was much higher, by roughly 24-fold, than that seen in *Task-1*$^{-/-}$ ($P < 0.001$) and 4-fold greater than that observed in *Task-3*$^{-/-}$ ($P < 0.02$). There was no significant difference in channel activity between *Task-1*$^{-/-}$ and *Task-3*$^{-/-}$ ($P = 0.19$) (Fig. 4*A*). The frequency of observation of TASK-like channel activity also differed between subject groups. Of patches formed (> 10 GΩ resistance), 82% of wild-type ($n = 45$; total patches: 55), 55% of *Task-1*$^{-/-}$ ($n = 44$; total patches: 80) and 68% of *Task-3*$^{-/-}$ ($n = 32$; total patches: 47) patches contained TASK-like channel activity (Fig. 4*B*).

The superimposition of scaled all-points histograms derived from control and knock-out type-1 cells generally resolved a clear separation of different amplitude peaks for the different genotypes. The superimposition of both single- and two-peaked wild-type all-points histograms with a *Task-1*$^{-/-}$ histogram placed the *Task-1*$^{-/-}$ peak clearly to the right of the wild-type peaks (Fig. 4*C* and *E*). Performing the same action with a *Task-3*$^{-/-}$ histogram saw the mutant peak align closely with the leftward peak in wild-type 'double peak' histograms at around 1.0–1.5 pA amplitude (Fig. 4*D*) and to the left of the principle peak in single-peaked histograms (Fig. 4*E*).

These data support the following conclusions: (i) the predominant form of background K^+-channel present in wild-type cells is a TASK-1/TASK-3 heteromultimer; (ii) the predominant form of background K^+-channel present in *Task-1*$^{-/-}$ cells is a TASK-3 homomultimer, and (iii) the predominant form of background K^+-channel present in *Task-3*$^{-/-}$ cells is a TASK-1 homomultimer (see Discussion).

Modulation of background channel activity

The oxygen sensitivity of background channel activity in rat type-1 cells has been well described (Buckler *et al.* 2000; Kim *et al.* 2009). It has also been demonstrated that rat type-1 cell background channels are strongly inhibited by metabolic poisons affecting oxidative phosphorylation (Williams & Buckler, 2004; Varas *et al.* 2007; Buckler, 2012). Little is known about the oxygen and metabolic sensitivity of wild-type TASK-1/TASK-3 channels in mouse type-1 cells or, indeed, of the sensitivities of the homomeric channels TASK-1 and TASK-3. The sensitivity of background/TASK K^+-channel activity to hypoxia and inhibitors of oxidative phosphorylation were therefore investigated.

Effects of hypoxia. Acute exposure to hypoxia was achieved using 100 mM K^+ HCO_3^- buffered Tyrode, pre-equilibrated with 5% CO_2 95% N_2. Exposure of isolated control mouse type-1 cells to hypoxia caused a rapid and reversible inhibition of single-channel activity, manifested as a general reduction in apparent noise when viewed on a long time base (Fig. 5*A*). Close examination of single-channel activity showed a decrease in multiple channel openings and a decreased frequency of single openings (Fig. 5*B*). All-points histograms revealed that hypoxia caused a decrease in frequency of all open channel current amplitudes, corresponding to a near uniform inhibition of background K^+-channel activity at all conductance levels (Fig. 5*C*). The main conductance state determined from all-points histograms was used independently to set 50% threshold levels for the determination of nP_{open} under normoxic and hypoxic conditions. In concordance with previous studies in rat type-1 cells, nP_{open} under hypoxia fell to a mean ± S.E.M. of 48.7 ± 4.3% of the normoxic control level ($n = 24$; $P < 0.001$, single-sample one-tailed *t* test) (Fig. 5*D*).

Examination of *Task-1*$^{-/-}$ type-1 cell patches revealed similar hypoxia-induced effects. Hypoxia brought about a rapid and reversible inhibition of TASK-3 K^+-channel activity (Fig. 5*E* and *F*), which was reflected by a lower frequency of current amplitudes corresponding to the main open level in all-points histograms (Fig. 5*G*). Under hypoxia nP_{open} fell significantly to 65.4 ± 6.8% of the normoxic control level ($n = 16$; $P < 0.001$, single-sample one-tailed *t* test) (Fig. 5*H*).

TASK-1 K^+-channel activity in *Task-3*$^{-/-}$ type-1 cells was similarly rapidly and reversibly inhibited by hypoxia (Fig. 5*I* and *J*). Under hypoxic conditions nP_{open} was reduced to 50.8 ± 12.3% of the normoxic value ($n = 9$; $P < 0.005$, single-sample one-tailed *t* test) (Fig. 5*L*). All-points histograms showed a decrease in frequency of single-channel current at all levels (Fig. 5*K*).

Effects of CN. The effects of cyanide on background channel activity were analogous to those of hypoxia as described above. Cyanide was added to high K^+ Tyrode as NaCN to a concentration of 2 mM. Superfusion

and outward currents were fitted independently by least squares linear regression and yielded a mean ± S.E.M. slope conductance of 37.6 ± 0.8 pS ($r^2 = 0.997$) for the inward current. *F*, mean single-channel *I–V* relationship for background channel activity in *Task-3*$^{-/-}$ type-1 cells ($n = 5$ for most points). Mean data for inward currents were fitted by least squares linear regression, which yielded a mean ± S.E.M. slope conductance of 18 ± 0.21 pS ($r^2 = 0.96$).

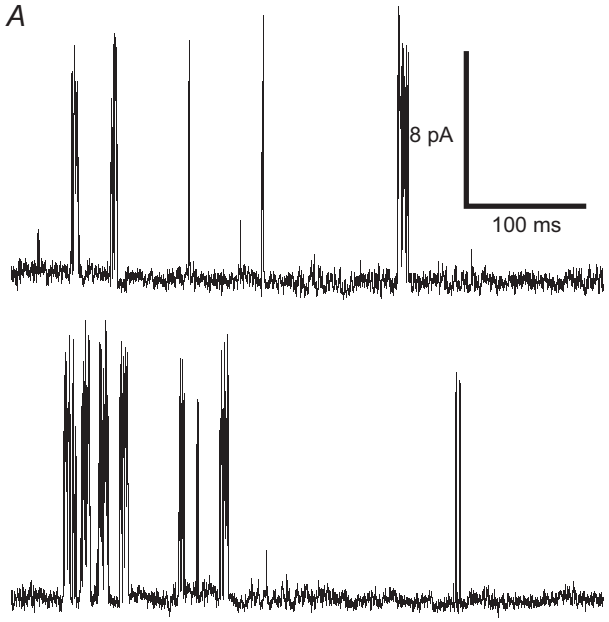

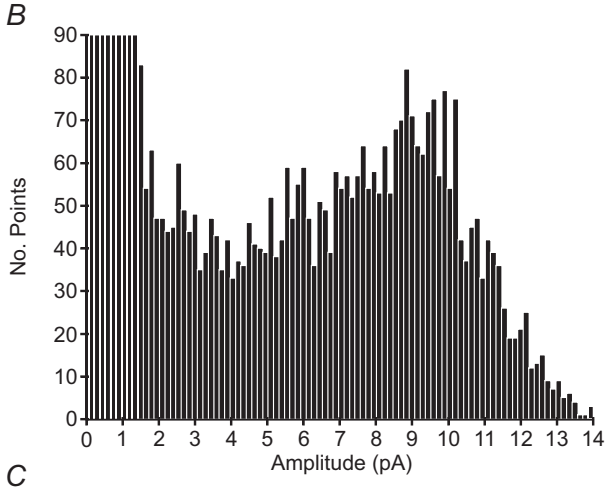

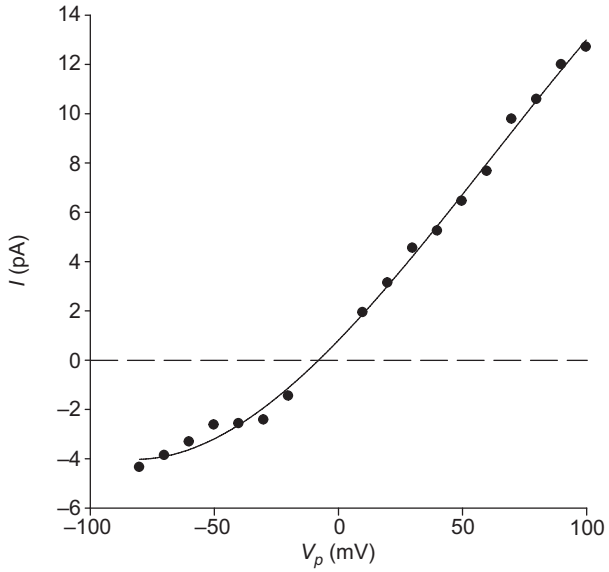

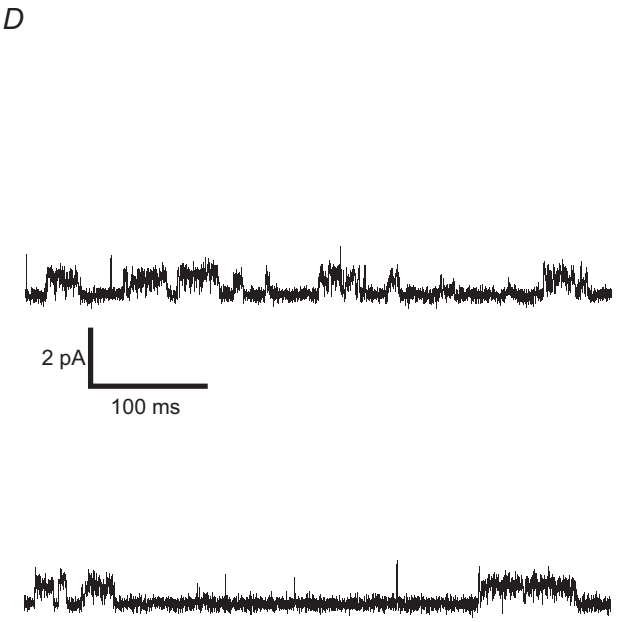

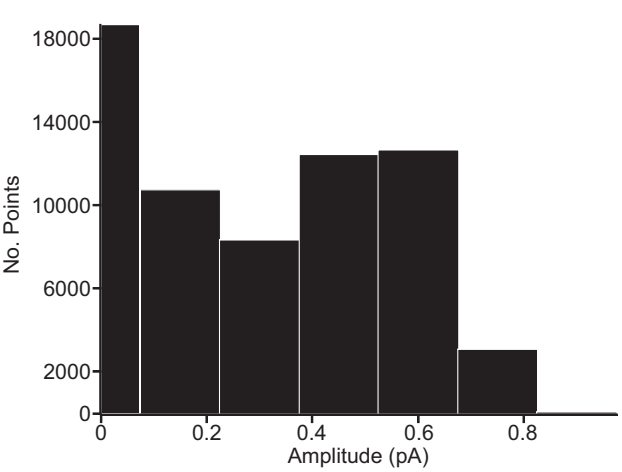

of wild-type type-1 cells with NaCN Tyrode caused a rapid inhibition of single-channel activity, which quickly recovered on return to standard Tyrode (Fig. 6*A* and *B*). These visual impressions were confirmed by the construction of all-points histograms, which showed a decrease in open-channel current across the whole range of amplitudes, corresponding to a near uniform inhibition of background K^+-channel activity at all conductance levels during NaCN exposure (Fig. 6*C*). Calculated nP_{open} values under NaCN exposure were $27.2 \pm 8.6\%$ of the control value ($n = 14$; $P < 0.001$, single-sample one-tailed *t* test) (Fig. 6*D*).

Exposure of *Task-1*$^{-/-}$ type-1 cells to NaCN caused a rapid and reversible inhibition of single-channel activity (Fig. 6*E* and *F*). Correspondingly, all-points histograms plotted from these data showed a decrease in frequency of current amplitudes corresponding to the main open state of TASK-3 (Fig. 6*G*). The effects of NaCN exposure on activity as determined by nP_{open} calculation appeared to be smaller than those observed in wild-type cells, with a fall in nP_{open} to $71.6 \pm 12.1\%$ of the control value ($n = 6$; $P < 0.05$, single-sample one-tailed *t* test) (Fig. 6*H*).

Background K^+-channel activity in *Task-3*$^{-/-}$ cells also appeared to be strongly inhibited by NaCN. In these type-1 cells, exposure to 2 mM NaCN caused a rapid and reversible decline in single-channel activity (Fig. 6*I* and *J*), with a corresponding decrease in the frequency of current amplitudes corresponding to TASK-1 open events as defined by all-points histograms (Fig. 6*K*). Using a 50% threshold derived from the main (TASK-1) conductance level, nP_{open} was calculated to fall to just $15.4 \pm 9.6\%$ of the control value ($n = 6$; $P < 0.001$, single-sample one-tailed *t* test) (Fig. 6*L*).

Effects of FCCP. When exposed to 1 μM FCCP (carbonyl cyanide 4-(trifluoromethoxy) phenylhydrazone), single-channel activity in wild-type cells rapidly decreased. Figure 7*A* shows an example of a multi-channel patch; note that FCCP caused a reduction in multiple and single opening events (Fig. 7*A* and *B*) as evidenced by the decline in frequency at all levels of channel current as shown in the all-points histogram (Fig. 7*C*). The main peak in the all-points histogram was used to set a 50% threshold from which nP_{open} was determined. FCCP decreased nP_{open} to just $13.4 \pm 4.2\%$ of the control value ($n = 13$; $P < 0.001$, single-sample one-tailed *t* test) (Fig. 7*D*). Background K^+-channel activity rapidly returned to control levels once the toxin was washed off. *Task-1*$^{-/-}$ type-1 cell background channel activity responded similarly, with a rapid reversible inhibition of channel activity by FCCP exposure (Fig. 7*E* and *F*). All-points histograms revealed a substantial decline in the frequency of current amplitudes corresponding to single TASK-3 channel activity (Fig. 7*G*). Examination of relative channel activity showed a reduction in nP_{open} during FCCP exposure to $57.3 \pm 9.3\%$ of the control value ($n = 14$; $P < 0.001$, single-sample one-tailed *t* test) (Fig. 7*H*).

Application of 1 μM FCCP to *Task-3*$^{-/-}$ type-1 cells caused an almost complete and reversible inhibition of single-channel activity (Fig. 7*I* and *J*). Histograms plotted from data recorded during FCCP exposure had little resolvable peak relative to controls (Fig. 7*K*), but the decline in the frequencies of current amplitudes relative to the control value was consistent with the inhibition of a TASK-1 channel. Quantification of this response to FCCP by calculation of nP_{open} revealed that activity was reduced to $31.9 \pm 10.3\%$ of the control value ($n = 8$; $P < 0.001$, paired one-tailed *t* test) (Fig. 7*L*).

Ca^{2+}-signalling in TASK knock-out cells

Having established that the oxygen-sensitive background K^+ currents are mediated by TASK-1/TASK-3 channels, we sought to observe the effects of genetic deletion of these channels on calcium signalling in isolated mouse type-1 cells. Baseline levels of calcium were measured in bicarbonate buffered Tyrode equilibrated with 20% oxygen, 5% CO_2 at pH 7.4 and 36°C in type-1 cells isolated from all four genotypes used in this study. Mean ± S.E.M. baseline $[Ca^{2+}]_i$ in wild-type cells was 112 ± 10 nM ($n = 9$). Similar levels were observed in *Task-1*$^{-/-}$ cells ($[Ca^{2+}]_i = 134 \pm 30$ nM; $n = 11$), *Task-3*$^{-/-}$ cells ($[Ca^{2+}]_i = 139 \pm 36$ nM; $n = 4$) and *Task-1*$^{-/-}$/*Task-3*$^{-/-}$ cells ($[Ca^{2+}]_i = 125 \pm 14$ nM; $n = 6$). None of the values obtained for baseline $[Ca^{2+}]_i$ in any of the knock-out genotypes were significantly different from that in wild-type cells.

Figure 3. Background channel activity in cell-attached *Task-1*$^{-/-}$/*Task-3*$^{-/-}$ patches
A, cell-attached recording of a large conductance channel in a *Task-1*$^{-/-}$/*Task-3*$^{-/-}$ type-1 cell. Two contiguous 500 ms sections of recording are shown. Recording conditions were as described in Fig. 1. *B*, all-points histogram generated from a 20 s segment of cell-attached recording under control conditions, with 150 fA bins. *C*, single-channel current–voltage (*I–V*) relationship for a large conductance channel present in a *Task-1*$^{-/-}$/*Task-3*$^{-/-}$ null type-1 cell ($n = 1$). Data for inward currents ($n = 2$) were fitted by least squares regression and yielded a mean ± S.E.M. slope conductance of 108 ± 4.8 pS ($r^2 = 0.987$). *D*, cell-attached recording of single-channel activity of a small conductance channel from a *Task-1*$^{-/-}$/*Task-3*$^{-/-}$ type-1 cell. *E*, all-points histogram generated from a 10 s segment of cell-attached recording under control conditions, with 150 fA bins. Calculation of single-channel conductance at 80 mV yielded a value of 7.5 pS.

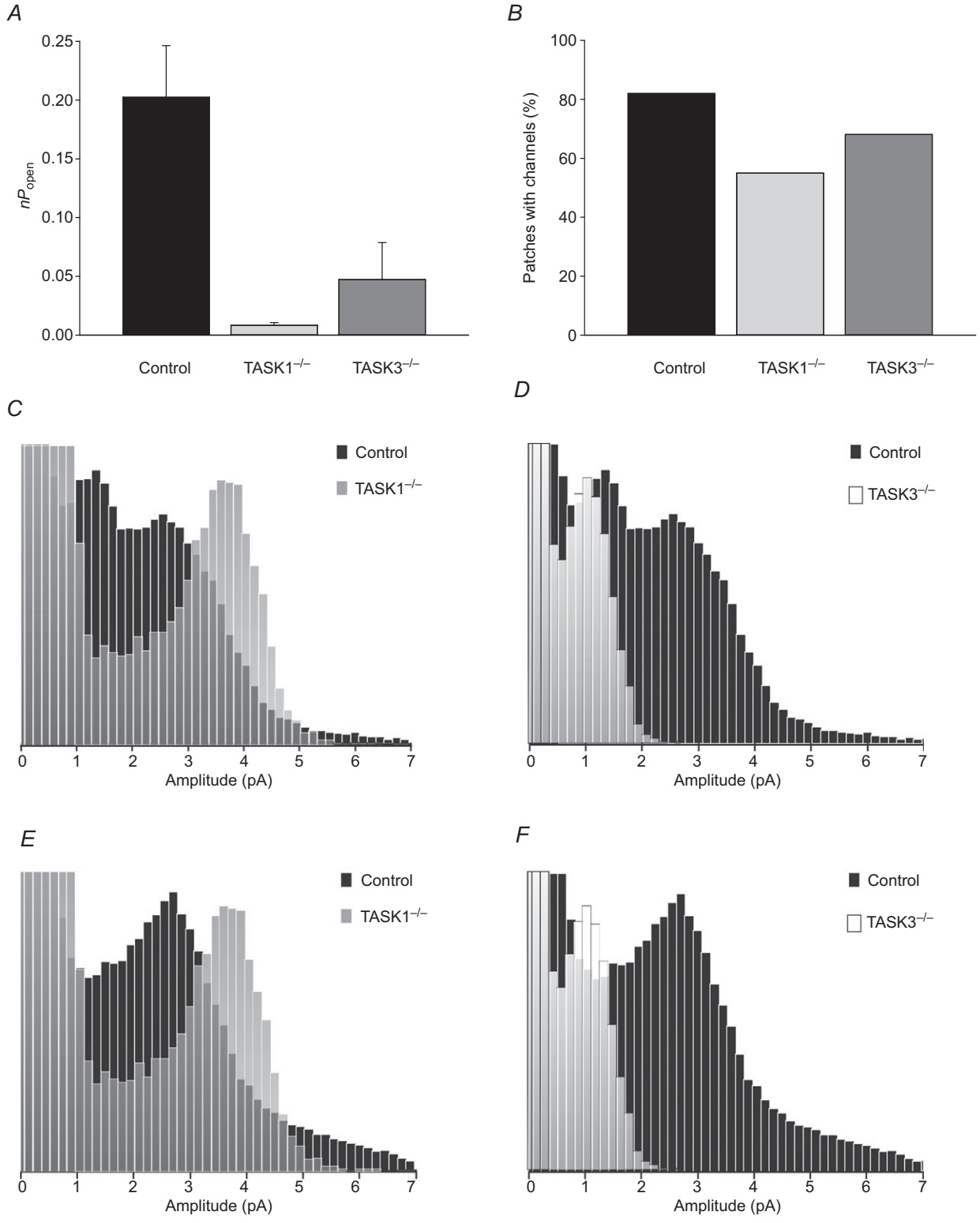

Figure 4. *Task-1*$^{-/-}$ and *Task-3*$^{-/-}$ single-channel summary
A, nP_{open} values for channel activity calculated under normoxic conditions at 80 mV V_p for control ($n = 30$), *Task-1*$^{-/-}$ ($n = 21$) and *Task-3*$^{-/-}$ ($n = 17$) type-1 cells. *B*, numbers of channel-containing patches as a percentage of total patches for control ($n = 45$), *Task-1*$^{-/-}$ ($n = 44$), and *Task-3*$^{-/-}$ ($n = 32$) cells. *C*, *D*, all-points histogram from a control type-1 cell with *Task-1*$^{-/-}$ and *Task-3*$^{-/-}$ superimposed, respectively. *E*, *F*, alternative all-points histogram from a control type-1 cell with *Task-1*$^{-/-}$ and *Task-3*$^{-/-}$, respectively. Note all histograms in this figure have been arbitrarily scaled such that peaks in the different histograms are of similar size.

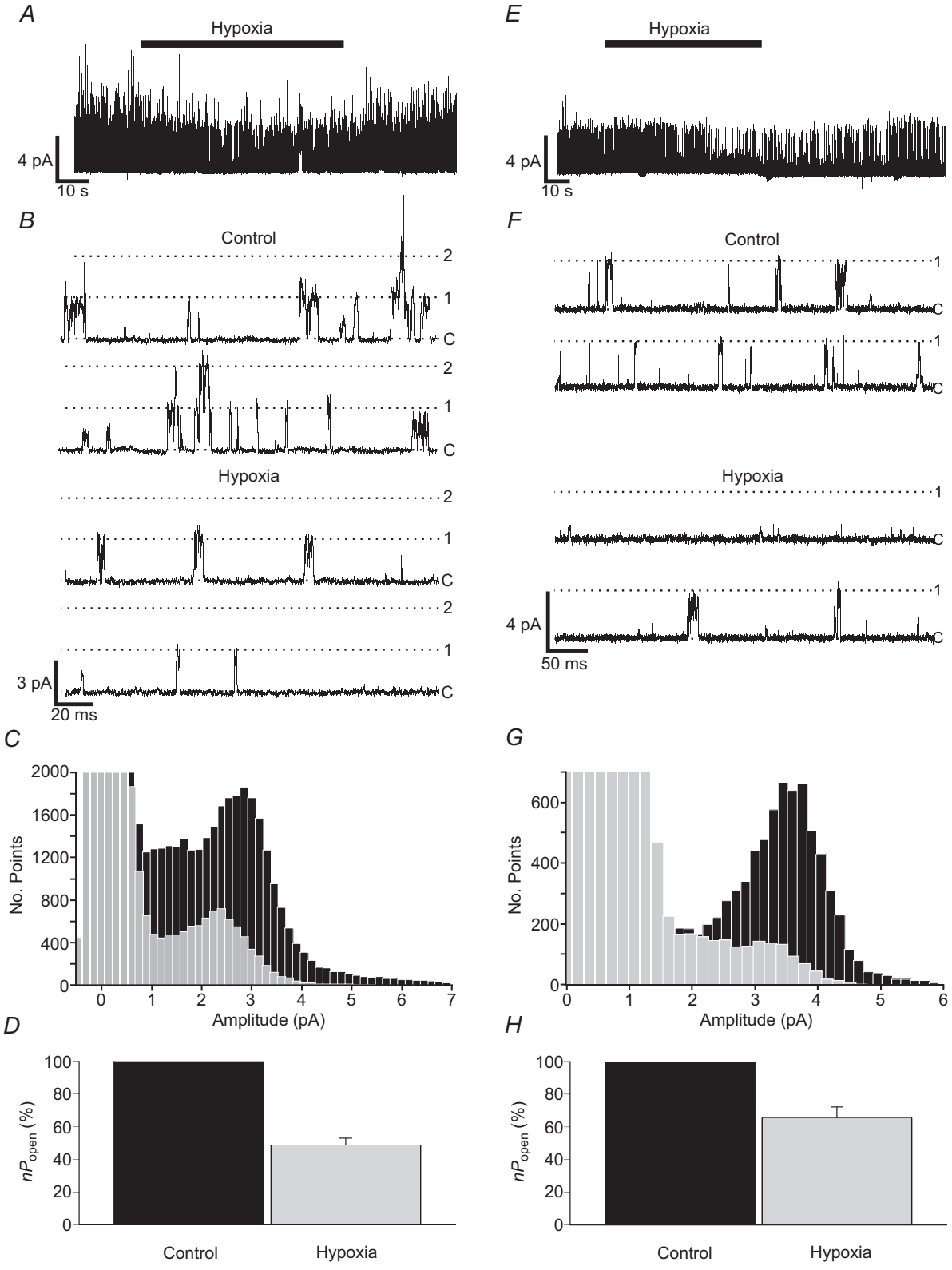

Figure 5. Oxygen sensitivity of TASK channels in type-1 cells
A, *B*, representative single-channel recording showing reversible inhibition of background channel activity by hypoxia in control type-1 cells. Cells were bathed in 100 mM K^+, nominally Ca^{2+}-free Tyrode solution. Hypoxia was induced by gassing Tyrode solutions with 5% CO_2 and 95% N_2. Pipette solution contained 140 mM K^+, with a pipette potential of +80 mV. *C*, superimposition of all-points histograms derived from recordings made

Type-1 cells were also exposed to hypoxia (95% N_2, 5% CO_2), which induced a brisk rise in $[Ca^{2+}]_i$ in wild-type cells ($\Delta[Ca^{2+}]_i$ 247 ± 54 nM; $n = 9$), *Task-1*$^{-/-}$ cells ($\Delta[Ca^{2+}]_i = 272 \pm 44$ nM; $n = 11$), *Task-3*$^{-/-}$ cells ($\Delta[Ca^{2+}]_i = 226 \pm 95$ nM; $n = 4$) and *Task-1*$^{-/-}$/*Task-3*$^{-/-}$ cells ($\Delta[Ca^{2+}]_i = 263 \pm 64$ nM; $n = 6$). In all instances the hypoxia-induced rise in $[Ca^{2+}]_i$ was substantially inhibited in calcium-free medium by 90 ± 6.5% ($n = 4$; $P < 0.001$) in control cells, 92 ± 2.7% ($n = 11$; $P < 0.001$) in *Task-1*$^{-/-}$ cells, 96 ± 2.0% ($n = 4$; $P < 0.001$) in *Task-3*$^{-/-}$ cells and 87 ± 4.7% ($n = 3$; $P < 0.002$, single-sample one-tailed *t* test) in *Task-1*$^{-/-}$/*Task-3*$^{-/-}$ cells (Fig. 8).

We further tested cells from all four genotypes for sensitivity to a variety of metabolic/mitochondrial inhibitors including cyanide (2 mM), rotenone and FCCP (both 1 μM). All three agents elicited a robust and statistically significant rise in $[Ca^{2+}]_i$ in type-1 cells from mice of all four genotypes ($P < 0.05$, assessed using a single-sample one-tailed *t* test on normalized data) (Fig. 8). There were no significant effects of genotype on responses to hypoxia, cyanide, rotenone and FCCP as assessed by two-way ANOVA.

Discussion

The aims of this study were to characterize background K^+-channels of the mouse type-1 cell, to establish the roles of *Task-1* and *Task-3* in forming these channels, and to investigate the hypoxia and metabolic sensitivity of any TASK channels present.

Characteristics of the K_B-channel in mouse type-1 cells

Cell-attached recordings from wild-type mouse type-1 cells revealed abundant single-channel activity at negative membrane potentials similar to that previously reported for K_B-channels in rat type-1 cells (Williams & Buckler, 2004) (Varas *et al.* 2007; Buckler, 2012) and to TASK-1 and TASK-3 fusion dimers expressed in HeLa cells (Kim *et al.* 2009). Mouse K_B-channels had flickery kinetics with short-lived open states and poorly defined or variable conductance levels, characteristics that are typical of rat K_B activity. Most all-points amplitude histograms typically displayed a single but broad peak at around 2.5 pA ($V_p = 80$ mV), suggesting one main, if ill-defined, open state.

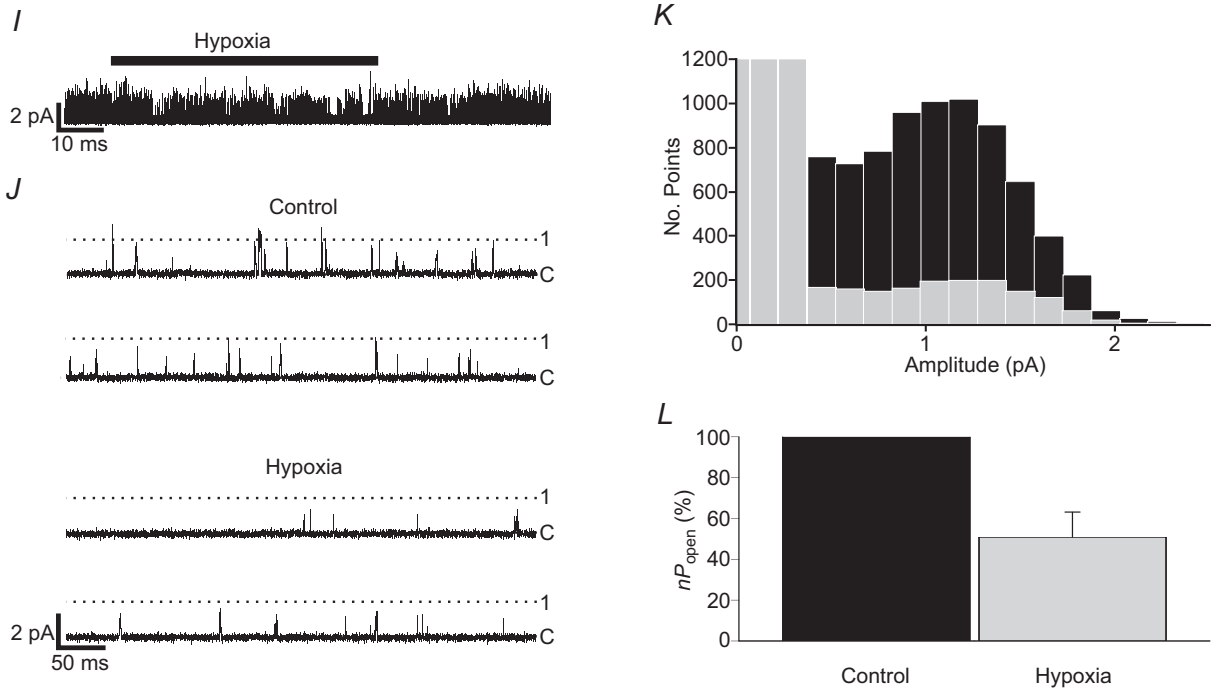

Figure 5.
under control and hypoxic conditions. *D*, comparison of background channel activity under control and hypoxic conditions ($n = 24$ patches). *E*, *F*, single-channel recording from a *Task-1*$^{-/-}$ type-1 cell showing the reversibility of inhibition of channel activity by hypoxia. *G*, superimposed histograms constructed from *Task-1*$^{-/-}$ data obtained under control and hypoxic conditions. *H*, relative channel activity for *Task-1*$^{-/-}$ under control and hypoxic conditions ($n = 16$ patches). *I*, *J*, *Task-3*$^{-/-}$ single-channel activity inhibition by hypoxia. *K*, superimposition of all-points histograms created from *Task-3*$^{-/-}$ type-1 cell control and hypoxia recordings. *L*, comparison of relative channel activity in *Task-3*$^{-/-}$ cells under control and hypoxic conditions ($n = 9$ patches).

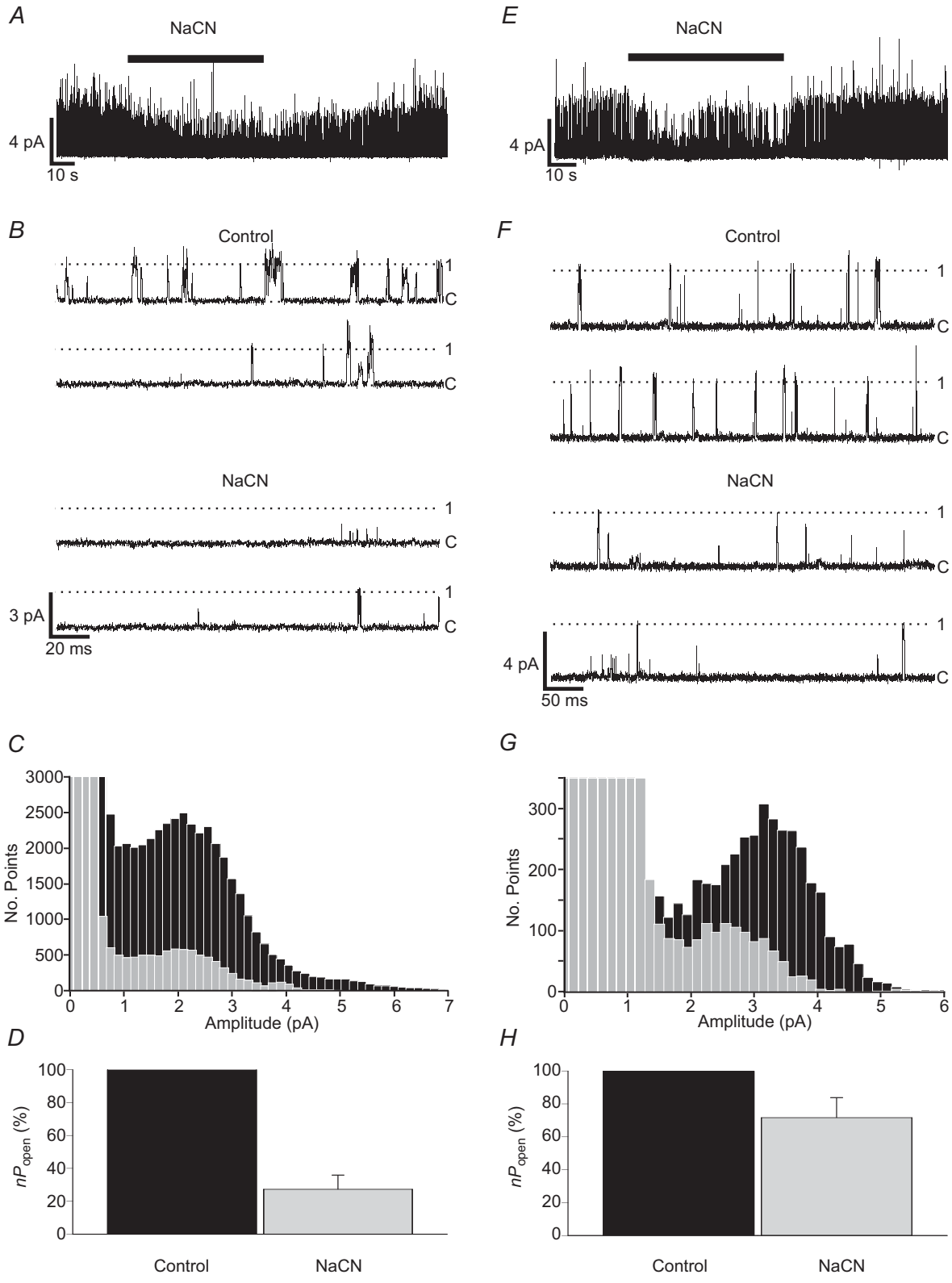

Figure 6. Cyanide sensitivity of TASK channels in type-1 cells
A, *B*, representative single-channel recording showing the reversible inhibition of background channel activity by 2 mM NaCN in control type-1 cells. Recording conditions were as in Fig. 5. *C*, superimposition of all-points histograms derived from recordings made during superfusion with control and cyanide Tyrode solutions. *D*, comparison of relative background channel activity in cell-attached patches under control and cyanide exposure

The K_B-channel is predominantly a TASK-1/TASK-3 heteromultimer

We investigated the molecular identity of the background K^+-channel in mice by using germline deletion of the two main candidate genes, *Task-1*$^{-/-}$ and *Task-3*$^{-/-}$. The first obvious difference between recordings from wild-type type-1 cells and those from either *Task-1*$^{-/-}$ or *Task-3*$^{-/-}$ mice is that channel activity was much lower in both of the knock-out strains. This manifested both as a reduction in mean nP_{open} for patches with channels and in the number of patches with any TASK-like channel activity. The second obvious difference is in the amplitude of single-channel current. In the *Task-1*$^{-/-}$ mouse, the main peak observed in all-points histograms occurred at a significantly higher current amplitude than that seen in the wild-type mouse, whereas in the *Task-3*$^{-/-}$ mouse it occurred at a much lower amplitude than in the wild-type mouse. The differences in single-channel current recorded at a pipette potential of +80 mV were mirrored by differences in the slope conductance in wild-type (33 pS), *Task-1*$^{-/-}$ (38 pS) and *Task-3*$^{-/-}$ (18 pS) mice. Thus disruption of either *Task-1* or *Task-3* reduces background K^+-channel activity substantially and fundamentally changes the biophysical properties of the remaining background K^+-channels, eliminating the 33 pS channel that predominates in the wild-type cell. Deletion of both *Task-1* and *Task-3* eliminated almost all K-channel activity at negative membrane potentials. The main form of background K^+-channel found in wild-type type-1 cells is therefore dependent upon functional copies of both *Task-1* and *Task-3* genes. These observations confirm that the predominant background K^+-channel present in wild-type type-1 cells is a heteromer of TASK-1 and TASK-3.

TASK-1 and TASK-3 homomers in *Task-3*$^{-/-}$ and *Task-1*$^{-/-}$ type-1 cells

The biophysical properties of the background K^+-channels remaining in single knock-out animals are comparable with those of TASK-1 and TASK-3 in heterologous expression systems [i.e. the main

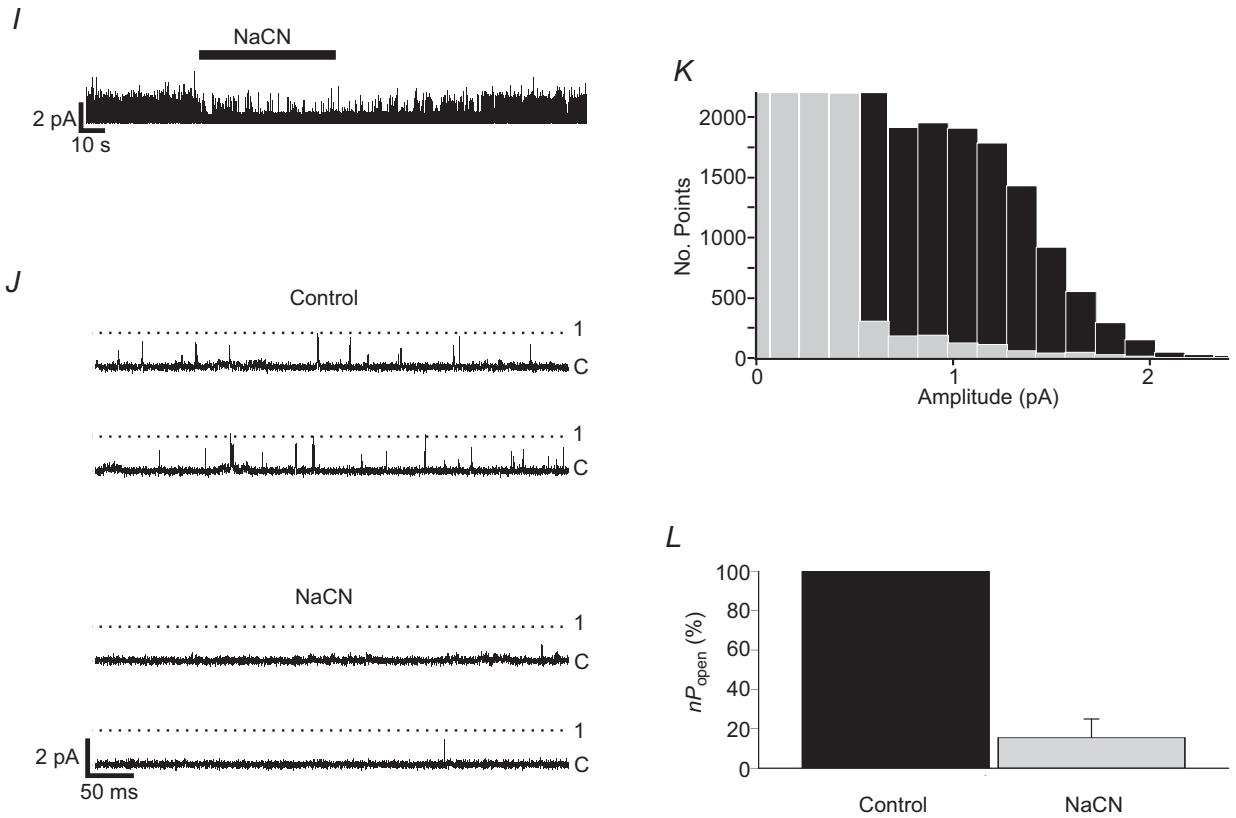

Figure 6.
($n = 14$ patches). *E*, *F*, single-channel recording from a *Task-1*$^{-/-}$ type-1 cell showing the effects of cyanide. *G*, superimposed histograms constructed from *Task-1*$^{-/-}$ data obtained during control and cyanide Tyrode superfusion. *H*, relative channel activity for *Task-1*$^{-/-}$ during control and cyanide exposure ($n = 6$ patches). *I*, *J*, *Task-3*$^{-/-}$ single-channel activity inhibition by cyanide. *K*, Superimposition of all-points histograms created from *Task-3*$^{-/-}$ type-1 cell control and cyanide recordings. *L*, comparison of relative channel activity in *Task-3*$^{-/-}$ cells during cyanide exposure ($n = 6$ patches).

conductance state in *Task-1*$^{-/-}$ cells is similar to that reported for TASK-3, 36 pS (Han *et al.* 2002)] and the main conductance state in *Task-3*$^{-/-}$ cells is similar to that reported for TASK-1 [16 pS (Kim *et al.* 1998; Leonoudakis *et al.* 1998; Patel *et al.* 1999)]. Moreover, both of these channels were absent from *Task-1*$^{-/-}$/T*ask-3*$^{-/-}$ double knock-out type-1 cells. We therefore conclude that the principle form of background K^+-channel activity in *Task-1*$^{-/-}$ type-1 cells is a TASK-3 homomer and that in *Task-3*$^{-/-}$ cells is a TASK-1 homomer.

Are homomeric forms of TASK-1 or TASK-3 also present in wild-type cells?

Kim *et al.* (2009) categorized three channel types in rat type-1 cells and attributed them to TASK-1, TASK-3 and TASK-1/TASK-3 heterodimers. An occasional feature ($n = 6$) of recordings from wild-type mouse type-1 cells was the appearance of a second peak in all-points histograms of conductance comparable with that in heterologously expressed TASK-1 and native TASK-1 channels in *Task-3*$^{-/-}$ mice. Although this may represent a sub-conductance state, the fact that its presence/activity relative to the main TASK-1/TASK-3 conductance state was highly variable between patches suggests it is more likely to reflect the presence of TASK-1 homomers in wild-type cells.

Although TASK-3 in *Task-1*$^{-/-}$ mice had a higher conductance than TASK-1/TASK-3 in wild-type cells,[1] we did not resolve any higher conductance peaks in all-points histograms compatible with TASK-3 channels being present in wild-type cells. This does not prove that TASK-3 homomers are totally absent, as a low level of activity may well be masked by the variable conductance levels of TASK-1/TASK-3, but it suggests that TASK-3 channel activity is not a prominent feature of mouse type-1 cells.

A conspicuous feature of both *Task-1*$^{-/-}$ and *Task-3*$^{-/-}$ type-1 cells was a much reduced level of channel activity compared with that in wild-type cells (average wild-type channel activity is 3.6-fold greater than the sum of channel activity in both single mutants). This is greater than might be expected from a simple gene dosage effect and may reflect a number of potential differences between heteromeric and homomeric forms of TASK, such as: (i) TASK-1/TASK-3 heteromers may be more readily assembled and/or trafficked to the plasma membrane than homomers; (ii) TASK-1/TASK-3 may be less prone to turnover, and (iii) TASK-1/TASK-3 channels may be intrinsically more active than homomeric channels. In respect of (i), it is worthy of note that TASK-1 (K2P3) and TASK-3 (K2P9) can also form heteromeric assemblies with TWIK (K2P1), which is often SUMOylated and the resultant TASK-1/TWIK-1 and TASK-3/TWIK-1 heterodimeric channels silenced (Plant *et al.* 2012). Thus, if heterodimer formation between TASK-1 and TASK-3 were favoured over other forms, the number of functional channels might be significantly greater in the wild-type than in either of the single knock-out cells. Such factors may also help to explain the relatively minor role played by homomeric forms of these channels in wild-type cells (Kim *et al.* 2009).

Other channel types present in type-1 cells

Recordings from *Task-1*$^{-/-}$/*Task-3*$^{-/-}$ type-1 cells revealed very little in the way of channel activity at negative membrane potentials of any description. This is in agreement with a substantive increase in input resistance for *Task-1*$^{-/-}$/*Task-3*$^{-/-}$ mouse type-1 cells (Ortega-Saenz *et al.* 2010). However, *Task-1*$^{-/-}$/*Task-3*$^{-/-}$ type-1 cells were not completely devoid of channel activity. The most conspicuous of the channels observed was a large conductance (108 pS) channel of low activity, which had characteristics similar to those of TREK/TRAAK channels in terms of conductance and flickery kinetics (Patel *et al.* 1998; Honore *et al.* 2002). TREK-1 mRNA and TRAAK immunoreactivity have both been found in type-1 cells (Yamamoto *et al.* 2002; Yamamoto & Taniguchi, 2006). This large conductance channel was also seen in seven patches from *Task-1*$^{-/-}$ mice and eight patches from *Task-3*$^{-/-}$ mice. We have not as yet observed this channel in type-1 cell patches from wild-type mice.

Another channel of lower conductance (approximately 7.5 pS) with long and very stable open states was also identified. This channel was found in all mouse genotypes studied and in rat type-1 cells (Buckler K.J., unpublished observations, 2013) and may be the same as an 8 pS channel briefly described by Kim *et al.* (2009). In a number of patches from knock-out genotypes, we also observed a small voltage-activated channel of approximately 1.4 pA at 80 mV V_p. Activity in this channel was low at negative membrane potentials, but increased by 13-fold upon depolarization (Fig. S1, online).

We did not observe any channel activity that could be ascribed to K_{ATP} channels, which have recently been reported in rat type-1 cells (Kim *et al.* 2011). However, we have previously seen such channels in rat type-1 cells in excised patches under certain conditions, albeit very rarely (K. J. Buckler, unpublished observations, 2001).

It should be noted that both TEA and 4-AP were included in our pipette-filling solution to help isolate TASK from other K^+-channels. As a consequence these

[1] Kim *et al.* (2009) did not observe an appreciable difference between the conductance of heterologously expressed TASK-3 and the TASK-1/3 fusion protein. This may be attributable to a genuine difference between naturally assembled TASK-1/TASK-3 heterodimers and TASK-1/3 fusion proteins, or it may reflect variations in ionic conditions, temperature or species.

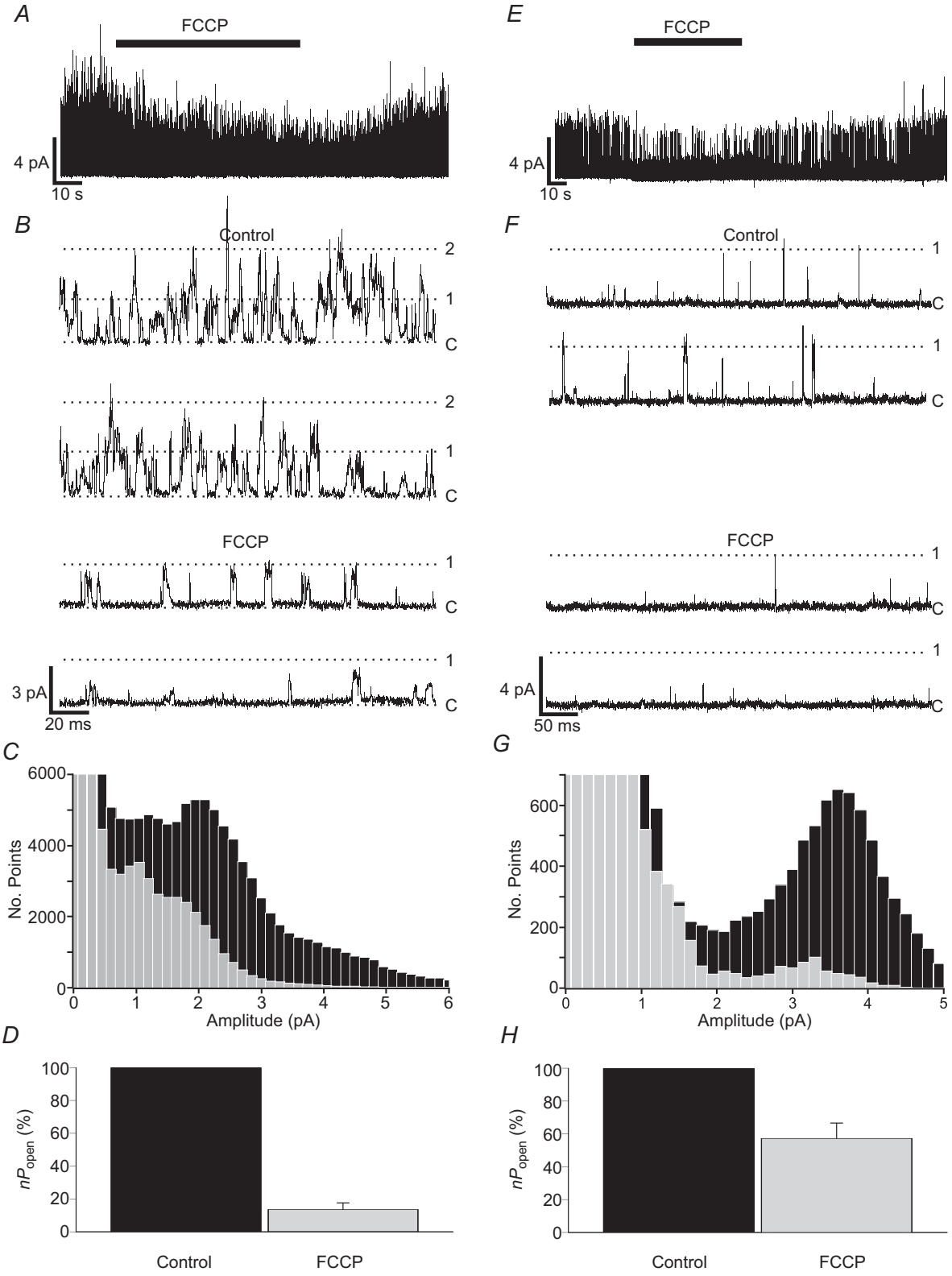

Figure 7. FCCP sensitivity of TASK-like channels in type-1 cells
A, *B*, representative single-channel recording showing the reversibility of inhibition of background channel activity by 1 μM FCCP in control type-1 cells. Recording conditions were as for hypoxia and cyanide experiments. *C*, superimposition of all-points histograms derived from recordings made during superfusion with control and FCCP Tyrode solutions. *D*, comparison of relative background channel activity in cell-attached patches during control

studies cannot be considered to represent a comprehensive survey of all the channels present in the membranes of type-1 cells. They do, however, confirm a lack of any significant background K^+-channel activity other than that which can be attributed to channels derived from *Task-1* and *Task-3*. We conclude therefore that, although other K^+-channels are present in these cells, the TEA and 4-AP insensitive background K^+ current seen in wild-type type-1 cells (Buckler, 1997) is primarily mediated by a TASK-1/TASK-3 heterodimer.

Effects of hypoxia and metabolic poisons on TASK channel activity

Hypoxia robustly inhibited background K^+-channel activity in wild-type cells at all conductance levels (Fig. 5*C*), which is consistent with an inhibition of the predominant TASK-1/TASK-3 heterodimeric channel, as well as any homomeric TASK-1 channels present. These results confirm previous observations in rat type-1 cells (Buckler *et al.* 2000; Kim *et al.* 2009). The inhibitory effects of hypoxia on K_B activity were recapitulated by the mitochondrial poisons NaCN (a complex IV inhibitor) and FCCP (an uncoupler), providing further evidence for the metabolic regulation of K_B activity (Buckler & Vaughan-Jones, 1998; Williams & Buckler, 2004; Wyatt & Buckler, 2004; Varas *et al.* 2007). Similar patterns of channel inhibition were also seen with hypoxia, CN and FCCP for TASK-1, in *Task-3*$^{-/-}$ type-1 cells, and TASK-3, in *Task-1*$^{-/-}$ type-1 cells. Thus TASK-1, TASK-3 and TASK-1/TASK-3 channels are all regulated by both hypoxia and metabolic inhibition. This suggests that either TASK-1 and TASK-3 share a common regulatory motif or they can assemble/interact with a common regulatory subunit which then couples them to oxygen and metabolic sensing pathways.

Although the qualitative effects of hypoxia and metabolic inhibitors on background channel activity were consistent between genotypes, a two-way ANOVA was carried out to determine whether there were any quantitative differences between genotypes or between stimuli (hypoxia, NaCN and FCCP). This analysis indicated that there was no significant interaction between the effects of genotype and stimuli on channel activity [$F(4, 101) = 1.997$, $P = 0.101$]. *Post hoc* analysis using Tukey's honestly significant differences (HSD) test did, however, indicate that the effects of both NaCN and FCCP were greater than those of hypoxia ($P < 0.02$ for

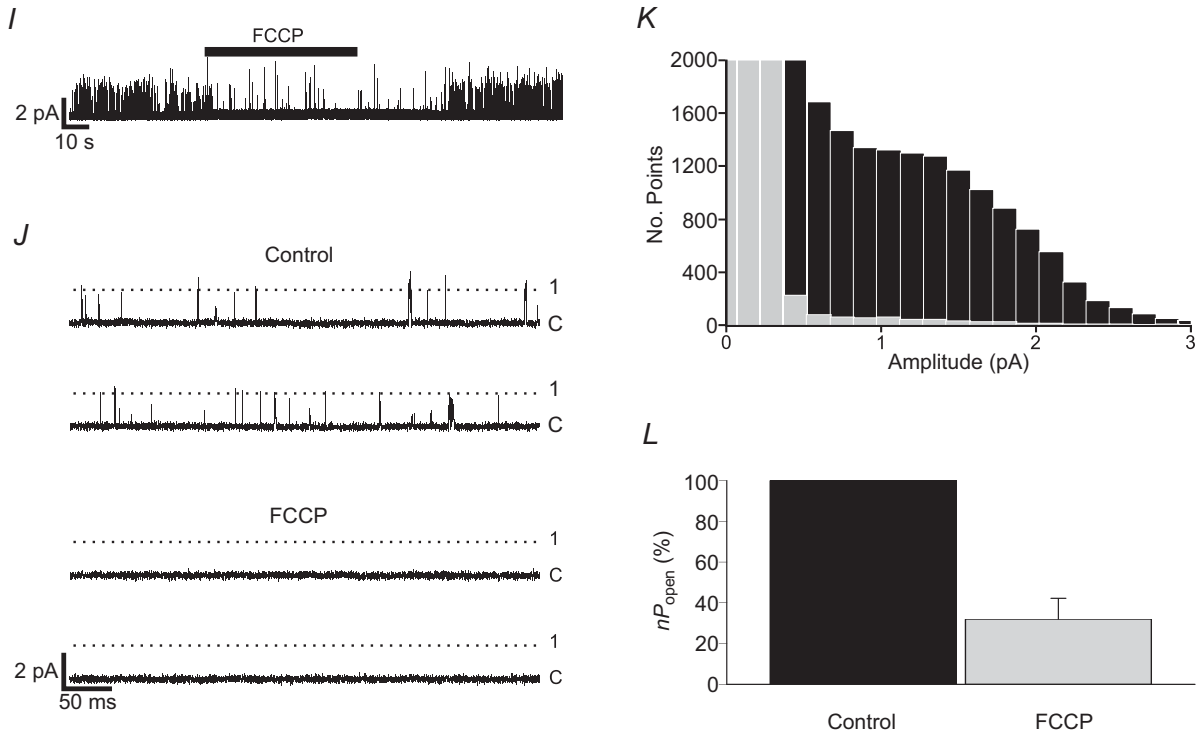

Figure 7.
and FCCP exposure ($n = 13$ patches). *E*, *F*, single-channel recording from a *Task-1*$^{-/-}$ type-1 cell showing the reversibility of inhibition of channel activity by FCCP. *G*, superimposed histograms constructed from *Task-1*$^{-/-}$ data obtained during control and FCCP Tyrode superfusion. *H*, relative channel activity for *Task-1*$^{-/-}$ during control and FCCP exposure ($n = 14$ patches). *I*, *J*, *Task-3*$^{-/-}$ single-channel activity inhibition by FCCP. *K*, superimposition of all-points histograms created from *Task-3*$^{-/-}$ type-1 cell control and FCCP recordings. *L*, comparison of relative channel activity in *Task-3*$^{-/-}$ cells during FCCP exposure ($n = 8$ patches).

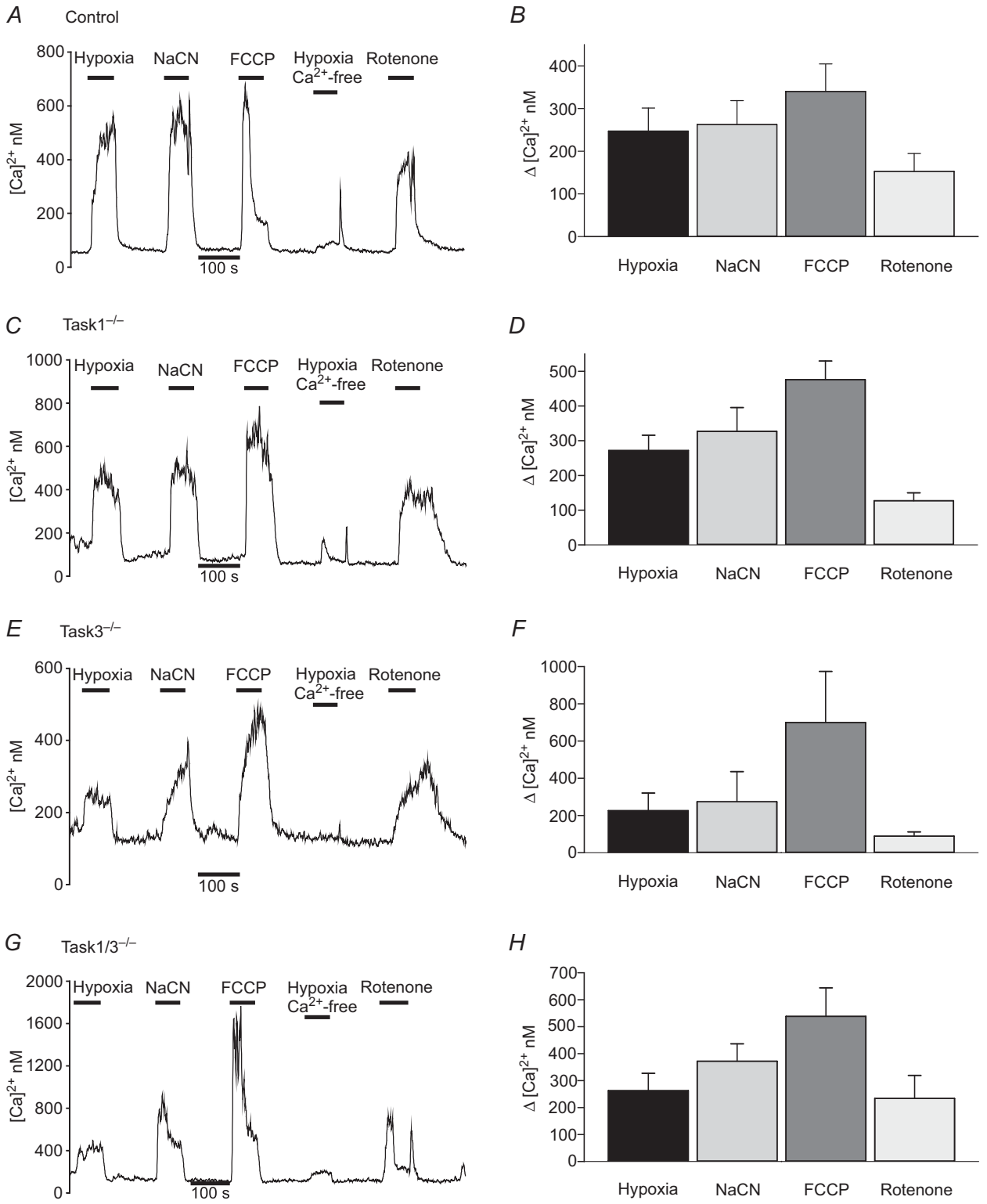

Figure 8. $[Ca^{2+}]_i$ signalling in wild-type and TASK knock-out type-1 cells
Individual recordings of intracellular $[Ca^{2+}]_i$ and summary data showing the effects of hypoxia, hypoxia in a Ca^{2+}-free Tyrode, NaCN (2 mM), FCCP (1 μM) and rotenone (1 μM) in type-1 cells from *A*, *B* wild-type mice, *C*, *D* *Task-1*$^{-/-}$ mice, *E*, *F* *Task-3*$^{-/-}$ mice, and *G*, *H* *Task-1*$^{-/-}$/*Task-3*$^{-/-}$ mice. Summary data are means ± standard error of the mean.

CN^- *vs.* hypoxia and $P < 0.01$ for FCCP *vs.* hypoxia) and that channel activity in *Task-1*$^{-/-}$ mice was less sensitive to stimuli than that in *Task-3*$^{-/-}$ or wild-type mice. Thus TASK-3 would seem to be less sensitive to inhibition by hypoxia and metabolic inhibitors than either TASK-1 or the TASK-1/TASK-3 heterodimer.

It seems increasingly probable that both oxygen sensing and metabolic sensing are linked in type-1 cells (Mulligan & Lahiri, 1982; Wyatt & Buckler, 2004). Indeed, it is possible that they are one and the same as mitochondrial function in type-1 cells is extraordinarily oxygen-sensitive (Duchen & Biscoe, 1992*a*,*b*; Buckler & Turner, 2013). Two potential mechanisms that may couple TASK channels to metabolism have thus far been described. One hypothesis proposes that channel activity is inhibited through phosphorylation by an AMP-activated protein kinase (AMPK) (Wyatt *et al.* 2007). However, only TASK-3, not TASK-1, appears to be regulated by AMPK (Dallas *et al.* 2009). Therefore, this pathway alone cannot account for the regulation of TASK-1 by hypoxia and metabolic inhibitors in *Task-3*$^{-/-}$ mice. Consequently, should AMPK be an essential link in the hypoxia transduction pathway, the actions of AMPK upon TASK-1 would need to be indirect. A second hypothesis rests on the observation that the wild-type TASK-1/TASK-3 channel of rat type-1 cells can be activated in the excised patch by mM levels of ATP (Varas *et al.* 2007), suggesting that changes in cytosolic ATP may directly modulate channel function. This property (of ATP sensitivity) has not yet been observed in heterologously expressed TASK-1 or TASK-3 and thus is presumably dependent on some as yet unidentified cofactor or accessory subunit. There may therefore be more to these channels in the form of regulatory subunits yet to be discovered.

Consequences of TASK channel deletion

In rat carotid body type-1 cells, TASK-like potassium channels are highly abundant and are believed to be responsible for the majority of background potassium conductance. Our studies in mice demonstrate that the major form of potassium channel activity present in wild-type cells at negative membrane potentials is a TASK-1/TASK-3 heterodimer and that in *Task-1*$^{-/-}$/*Task-3*$^{-/-}$ mice, background K-channel activity is very much reduced. This conclusion is supported by whole cell recordings that show a substantial decrease in resting membrane conductance in *Task-1*$^{-/-}$/*Task-3*$^{-/-}$ mice (Ortega-Saenz *et al.* 2010). Given the fundamental importance of background K^+ currents in setting resting membrane potential, the loss of TASK-1 and TASK-3 would be expected to result in a sustained depolarization of type-1 cells and a consequent increase in resting $[Ca^{2+}]_i$. Yet resting $[Ca^{2+}]_i$ levels were similar in all genotypes. Ortega-Saenz *et al.* (2010) similarly reported that resting membrane potential was only slightly depolarized in type-1 cells from *Task-1*$^{-/-}$/*Task-3*$^{-/-}$ mice. These data contrast strikingly with the effects of acute inhibition of background K currents by physiological stimuli, chemical stimuli or pharmacological inhibition with Ba^{2+}, all of which cause much greater depolarization and a very marked increase in intracellular calcium (Buckler & Vaughan Jones, 1994*b*; Buckler & Vaughan-Jones, 1998; Buckler, 1999; Wyatt & Buckler, 2004). This indicates that in the setting of germline deletion of *Task-1* and *Task-3*, the depolarizing effects of the loss of background K^+-channel activity must be compensated for. As the resting membrane potential represents a balance between passive outward potassium current plus outward Na^+-pump current against inward current generated by the passive influx of other cations (e.g. Na^+ and Ca^{2+}) and/or efflux of anions, any loss of background potassium current could be compensated for by changes in permeability to these other ions and/or electrogenic transporter activity. These other background currents are as yet poorly defined in the type-1 cell, but a substantial resting sodium current has been identified (Buckler, 1997; Carpenter & Peers, 2001). A further contributory factor in respect of the limited depolarization reported in type-1 cells from *Task-1*$^{-/-}$/*Task-3*$^{-/-}$ mice may be the accompanying decrease in voltage-gated Ca^{2+} current density (Ortega-Saenz *et al.* 2010). Voltage-gated Ca^{2+} currents tend to become active at potentials positive to −50 mV with significant Ca^{2+} influx or Ca^{2+} current often evident at −40 mV (Urena *et al.* 1989; Buckler & Vaughan Jones, 1994*a*; Silva & Lewis, 1995). Voltage-gated Ca^{2+} current would therefore normally add to the depolarizing effects of background inward currents once membrane potential becomes positive to approximately −50 mV.

The idea that germline deletion of TASK-channels leads to compensatory changes in the expression and/or activity of other ion channels is supported not only by observed changes in voltage-gated Ca^{2+} and $-K^+$ currents in *Task-1*$^{-/-}$/*Task-3*$^{-/-}$ type-1 cells (Ortega-Saenz *et al.* 2010), but also by studies in other cells in which the knock-out of TASK channels has resulted in the upregulation of GABA(A) receptors in the brain (Linden *et al.* 2008). These observations make clear the difficulties inherent in attempts to determine the normal physiological role of any ion channel by gene deletion.

We also noted significant chemosensitivity, measured as an increase in $[Ca^{2+}]_i$, to both hypoxia and a range of metabolic inhibitors in all TASK knock-out cells. In *Task-1*$^{-/-}$ and *Task-3*$^{-/-}$ cells, this could be explained by the fact that the remaining homomeric forms of TASK-3 and TASK-1 retain sensitivity to both hypoxia and metabolic inhibitors. In the case of the double knock-out, however, the obvious implication is that there must be other currents present in the type-1 cells of *Task-1*$^{-/-}$/*Task-3*$^{-/-}$ mice that are capable of

being regulated by hypoxia and metabolic inhibitors. Large-conductance calcium-activated potassium channels (BK_{Ca}) have been reported to be oxygen- and cyanide-sensitive in rat type-1 cells (Peers, 1990; Peers & O'Donnell, 1990; Lopez Lopez *et al.* 1997), but paxilline, an inhibitor of BK_{Ca}, failed to mimic or alter the secretory responses to hypoxia in *Task-1*$^{-/-}$/*Task-3*$^{-/-}$ mice (Ortega-Saenz *et al.* 2010). Voltage-activated potassium channels (K_V) have been reported to be oxygen-sensitive in the mouse (Perez Garcia *et al.* 2004; Yamaguchi *et al.* 2004), but their activation threshold, particularly in the *Task-1*$^{-/-}$/*Task-3*$^{-/-}$ type-1 cell, seems to be quite low (i.e. positive to −30 mV) (Perez Garcia *et al.* 2004; Ortega-Saenz *et al.* 2010). It would thus seem unlikely that oxygen-sensitive BK_{Ca} and/or K_v channels can account for hypoxic excitation of *Task-1*$^{-/-}$/*Task-3*$^{-/-}$ type-1 cells. Consequently, our data suggest the presence of novel, as yet unidentified, oxygen- and metabolism-sensitive ionic currents in the type-1 cell. We did observe oxygen sensitivity in one patch from *Task-1*$^{-/-}$/*Task-3*$^{-/-}$ cells in what appeared to be a larger conductance (TREK-like) channel and therefore other background K-channels may be oxygen-sensitive in these cells. Given the low level of background K-channel activity in *Task-1*$^{-/-}$/*Task-3*$^{-/-}$ type-1 cells, however, any small oxygen-sensitive inward current, or possibly the inhibition of an outward pump current, may be sufficient to depolarize and excite these cells. Such currents could easily have been overlooked in previous studies, given the magnitude of the resting K-conductance in wild-type cells. We note from previous studies that the reversal potentials for oxygen-sensitive background currents in rat type-1 cells do not always coincide exactly with those of background K-channel inhibitors (see Fig. 2 in Buckler *et al.* 2000), which may indicate the presence of an oxygen-sensitive inward current. *Task-1*$^{-/-}$/*Task-3*$^{-/-}$ mice may therefore provide a useful model in which to look for small, novel oxygen-sensitive currents in type-1 cells.

Conclusions

Despite the present considerations regarding the possible existence of other oxygen-sensitive currents in type-1 cells, it is clear from electrophysiological investigations that in normal cells inhibition of a background K current is a major contributor to membrane depolarization in response to both hypoxia and acidosis (Buckler, 1997; Buckler *et al.* 2000). Our data now confirm that this background K^+ current in carotid body type-1 cells is predominantly carried via TASK-1/TASK-3 heterodimeric channels with a lesser contribution from TASK-1 homomeric channels. All three types of channel (TASK-1, TASK-3 and TASK-1/TASK-3) are sensitive to hypoxia and metabolic inhibitors, but the most sensitive seem to be those containing the TASK-1 subunit.

References

Aller MI, Veale EL, Linden AM, Sandu C, Schwaninger M, Evans LJ, Korpi ER, Mathie A, Wisden W & Brickley SG (2005). Modifying the subunit composition of TASK channels alters the modulation of a leak conductance in cerebellar granule neurons. *J Neurosci* **25**, 11455–11467.

Brickley SG, Aller MI, Sandu C, Veale EL, Alder FG, Sambi H, Mathie A & Wisden W (2007). TASK-3 two-pore domain potassium channels enable sustained high-frequency firing in cerebellar granule neurons. *J Neurosci* **27**, 9329–9340.

Brohawn SG, del Marmol J & MacKinnon R (2012). Crystal structure of the human K2P TRAAK, a lipid- and mechano-sensitive K^+ ion channel. *Science* **335**, 436–441.

Buckler KJ (1997). A novel oxygen-sensitive potassium current in rat carotid body type I cells. *J Physiol* **498**, 649–662.

Buckler KJ (1999). Background leak K^+-currents and oxygen sensing in carotid body type 1 cells. *Respir Physiol* **115**, 179–187.

Buckler KJ (2012). Effects of exogenous hydrogen sulphide on calcium signalling, background (TASK) K channel activity and mitochondrial function in chemoreceptor cells. *Pflugers Arch* **463**, 743–754.

Buckler KJ & Turner PJ (2013). Oxygen sensitivity of mitochondrial function in rat arterial chemoreceptor cells. *J Physiol* **591**, 3549–3563.

Buckler KJ & Vaughan-Jones RD (1998). Effects of mitochondrial uncouplers on intracellular calcium, pH and membrane potential in rat carotid body type I cells. *J Physiol* **513**, 819–833.

Buckler KJ & Vaughan Jones RD (1993). Effects of acidic stimuli on intracellular calcium in isolated type I cells of the neonatal rat carotid body. *Pflugers Arch* **425**, 22–27.

Buckler KJ & Vaughan Jones RD (1994*a*). Effects of hypercapnia on membrane potential and intracellular calcium in rat carotid body type I cells. *J Physiol* **478**, 157–171.

Buckler KJ & Vaughan Jones RD (1994*b*). Effects of hypoxia on membrane potential and intracellular calcium in rat neonatal carotid body type I cells. *J Physiol* **476**, 423–428.

Buckler KJ, Williams BA & Honore E (2000). An oxygen-, acid- and anaesthetic-sensitive TASK-like background potassium channel in rat arterial chemoreceptor cells. *J Physiol* **525**, 135–142.

Carpenter E & Peers C (2001). A standing Na^+ conductance in rat carotid body type I cells. *Neuroreport* **12**, 1421–1425.

Chapman CG, Meadows HJ, Godden RJ, Campbell DA, Duckworth M, Kelsell RE, Murdock PR, Randall AD, Rennie GI & Gloger IS (2000). Cloning, localization and functional expression of a novel human, cerebellum specific, two pore domain potassium channel. *Brain Res Mol Brain Res* **82**, 74–83.

Czirjak G & Enyedi P (2002). Formation of functional heterodimers between the TASK-1 and TASK-3 two-pore domain potassium channel subunits. *J Biol Chem* **277**, 5426–5432.

Dallas ML, Scragg JL, Wyatt CN, Ross F, Hardie DG, Evans AM & Peers C (2009). Modulation of O_2 sensitive K^+ channels by AMP-activated protein kinase. *Adv Exp Med Biol* **648**, 57–63.

Duchen MR & Biscoe TJ (1992*a*). Mitochondrial function in type I cells isolated from rabbit arterial chemoreceptors. *J Physiol* **450**, 13–31.

Duchen MR & Biscoe TJ (1992*b*). Relative mitochondrial membrane potential and $[Ca^{2+}]_i$ in type I cells isolated from the rabbit carotid body. *J Physiol* **450**, 33–61.

e Silva MJ & Lewis DL (1995). L- and N-type Ca^{2+} channels in adult rat carotid body chemoreceptor type I cells. *J Physiol* **489**, 689–699.

Evans AM, Mustard KJ, Wyatt CN, Peers C, Dipp M, Kumar P, Kinnear NP & Hardie DG (2005). Does AMP-activated protein kinase couple inhibition of mitochondrial oxidative phosphorylation by hypoxia to calcium signaling in O_2-sensing cells? *J Biol Chem* **280**, 41504–41511.

Goldstein SA, Price LA, Rosenthal DN & Pausch MH (1996). ORK1, a potassium-selective leak channel with two pore domains cloned from *Drosophila melanogaster* by expression in *Saccharomyces cerevisiae*. *Proc Natl Acad Sci U S A* **93**, 13256–13261.

Han J, Truell J, Gnatenco C & Kim D (2002). Characterization of four types of background potassium channels in rat cerebellar granule neurons. *J Physiol* **542**, 431–444.

Honore E, Maingret F, Lazdunski M & Patel AJ (2002). An intracellular proton sensor commands lipid- and mechano-gating of the K^+ channel TREK-1. *EMBO J* **21**, 2968–2976.

Kang D, Han J, Talley EM, Bayliss DA & Kim D (2004). Functional expression of TASK-1/TASK-3 heteromers in cerebellar granule cells. *J Physiol* **554**, 64–77.

Kim D, Cavanaugh EJ, Kim I & Carroll JL (2009). Heteromeric TASK-1/TASK-3 is the major oxygen-sensitive background K^+ channel in rat carotid body glomus cells. *J Physiol* **587**, 2963–2975.

Kim D, Fujita A, Horio Y & Kurachi Y (1998). Cloning and functional expression of a novel cardiac two-pore background K^+ channel (cTBAK-1). *Circ Res* **82**, 513–518.

Kim D, Kim I, Papreck JR, Donnelly DF & Carroll JL (2011). Characterization of the ATP-sensitive K^+ channel in the rat carotid body glomus cells. *Respir Physiol Neurobiol* **177**, 247–255.

Kim Y, Bang H & Kim D (2000). TASK-3, a new member of the tandem pore K^+ channel family. *J Biol Chem* **275**, 9340–9347.

Leonoudakis D, Gray AT, Winegar BD, Kindler CH, Harada M, Taylor DM, Chavez RA, Forsayeth JR & Yost CS (1998). An open rectifier potassium channel with two pore domains in tandem cloned from rat cerebellum. *J Neurosci* **18**, 868–877.

Lesage F, Guillemare E, Fink M, Duprat F, Lazdunski M, Romey G & Barhanin J (1996*a*). TWIK-1, a ubiquitous human weakly inward rectifying K^+ channel with a novel structure. *EMBO J* **15**, 1004–1011.

Lesage F, Reyes R, Fink M, Duprat F, Guillemare E & Lazdunski M (1996*b*). Dimerization of TWIK-1 K^+ channel subunits via a disulfide bridge. *EMBO J* **15**, 6400–6407.

Linden AM, Aller MI, Leppa E, Rosenberg PH, Wisden W & Korpi ER (2008). K^+ channel TASK-1 knockout mice show enhanced sensitivities to ataxic and hypnotic effects of GABA(A) receptor ligands. *J Pharmacol Exp Ther* **327**, 277–286.

Lopez Lopez JR, Gonzalez C & Perez Garcia MT (1997). Properties of ionic currents from isolated adult rat carotid body chemoreceptor cells: effect of hypoxia. *J Physiol* **499**, 429–441.

Miller AN & Long SB (2012). Crystal structure of the human two-pore domain potassium channel K2P1. *Science* **335**, 432–436.

Mulligan E & Lahiri S (1982). Separation of carotid body chemoreceptor responses to O_2 and CO_2 by oligomycin and by antimycin A. *Am J Physiol Cell Physiol* **242**, C200–C206.

Ortega-Saenz P, Levitsky KL, Marcos-Almaraz MT, Bonilla-Henao V, Pascual A & Lopez-Barneo J (2010). Carotid body chemosensory responses in mice deficient of TASK channels. *J Gen Physiol* **135**, 379–392.

Patel AJ, Honore E, Lesage F, Fink M, Romey G & Lazdunski M (1999). Inhalational anesthetics activate two-pore-domain background K^+ channels. *Nat Neurosci* **2**, 422–426.

Patel AJ, Honore E, Maingret F, Lesage F, Fink M, Duprat F & Lazdunski M (1998). A mammalian two pore domain mechano-gated S-like K^+ channel. *EMBO J* **17**, 4283–4290.

Peers C (1990). Hypoxic suppression of K^+ currents in type I carotid body cells: selective effect on the Ca^{2+}-activated K^+ current. *Neurosci Lett* **119**, 253–256.

Peers C & O'Donnell J (1990). Potassium currents recorded in type I carotid body cells from the neonatal rat and their modulation by chemoexcitatory agents. *Brain Res* **522**, 259–266.

Perez Garcia MT, Colinas O, Miguel Velado E, Moreno Dominguez A & Lopez Lopez JR (2004). Characterization of the Kv channels of mouse carotid body chemoreceptor cells and their role in oxygen sensing. *J Physiol* **557**, 457–471.

Plant LD, Zuniga L, Araki D, Marks JD & Goldstein SA (2012). SUMOylation silences heterodimeric TASK potassium channels containing K2P1 subunits in cerebellar granule neurons. *Sci Signal* **5**, 84.

Rajan S, Wischmeyer E, Xin Liu G, Preisig Muller R, Daut J, Karschin A & Derst C (2000). TASK-3, a novel tandem pore domain acid-sensitive K^+ channel. An extracellular histiding as pH sensor. *J Biol Chem* **275**, 16650–16657.

Trapp S, Aller MI, Wisden W & Gourine AV (2008). A role for TASK-1 (KCNK3) channels in the chemosensory control of breathing. *J Neurosci* **28**, 8844–8850.

Urena J, Lopez Lopez J, Gonzalez C & Lopez Barneo J (1989). Ionic currents in dispersed chemoreceptor cells of the mammalian carotid body. *J Gen Physiol* **93**, 979–999.

Varas R, Wyatt CN & Buckler KJ (2007). Modulation of TASK-like background potassium channels in rat arterial chemoreceptor cells by intracellular ATP and other nucleotides. *J Physiol* **583**, 521–536.

Williams BA & Buckler KJ (2004). Biophysical properties and metabolic regulation of a TASK-like potassium channel in rat carotid body type 1 cells. *Am J Physiol Lung Cell Mol Physiol* **286**, L221–L230.

Wyatt CN & Buckler KJ (2004). The effect of mitochondrial inhibitors on membrane currents in isolated neonatal rat carotid body type I cells. *J Physiol* **556**, 175–191.

Wyatt CN & Evans AM (2007). AMP-activated protein kinase and chemotransduction in the carotid body. *Respir Physiol Neurobiol* **157**, 22–29.

Wyatt CN, Mustard KJ, Pearson SA, Dallas ML, Atkinson L, Kumar P, Peers C, Hardie DG & Evans AM (2007). AMP-activated protein kinase mediates carotid body excitation by hypoxia. *J Biol Chem* **282**, 8092–8098.

Yamaguchi S, Lande B, Kitajima T, Hori Y & Shirahata M (2004). Patch clamp study of mouse glomus cells using a whole carotid body. *Neurosci Lett* **357**, 155–157.

Yamamoto K, Kummer W, Atoji Y & Suzuki Y (2002). TASK-1, TASK-2, TASK-3 and TRAAK immunoreactivities in the rat carotid body. *Brain Research* **950**, 304–307.

Yamamoto Y & Taniguchi K (2006). Expression of tandem P domain K^+ channel, TREK-1, in the rat carotid body. *J Histochem Cytochem* **54**, 467–472.

Additional information

Competing interests

None declared.

Author contributions

All experiments were performed in the Department of Physiology, Anatomy and Genetics, University of Oxford. K.J.B. and P.J.T. conceived and designed the experiments. P.J.T. performed the experiments, collected data, and was primarily responsible for data analysis. K.J.B. and P.J.T. interpreted the data, K.J.B. drafted the manuscript and both authors participated in the critical review and revision of the manuscript for important intellectual content. Both authors have read and approved the final submitted version of this manuscript.

Funding

This work was funded by a British Heart Foundation project grant (PG/08/086/25849) and a Medical Research Council UK project grant (G101134).

Acknowledgements

We would like to thank Professor William Wisden and Dr Stefan Trapp for the generous gifts of *Task-1*$^{-/-}$ and *Task-3*$^{-/-}$ mice. We would also like to thank Denise Jelfs for assistance and advice in maintaining the transgenic mouse lines used in this study.